The Astrophysical Journal, 754:130 (17pp), 2012 August 1 doi:10.1088/0004-637X/754/2/130


# STAR FORMATION HISTORY IN TWO FIELDS OF THE SMALL MAGELLANIC CLOUD BAR*

M. Cignoni[1,2], A. A. Cole[3], M. Tosi[2], J. S. Gallagher[4], E. Sabbi[5], J. Anderson[5], E. K. Grebel[6], and A. Nota[5]
[1] Dipartimento di Astronomia, Universitá degli Studi di Bologna, via Ranzani, I-40127 Bologna, Italy; michele.cignoni@unibo.it
[2] Istituto Nazionale di Astrofisica, Osservatorio Astronomico di Bologna, Via Ranzani 1, I-40127 Bologna, Italy
[3] School of Mathematics and Physics, University of Tasmania, Private Bag 37, Hobart, Tasmania 7001, Australia
[4] Department of Astronomy, University of Wisconsin, 475 North Charter Street, Madison, WI 53706, USA
[5] STScI, Baltimore, MD 21218, USA
[6] Astronomisches Rechen-Institut, Zentrum für Astronomie der Universität Heidelberg, Mönchhofstr. 12-14, 69120 Heidelberg, Germany
*Received 2012 April 7; accepted 2012 May 31; published 2012 July 17*

## ABSTRACT

The Bar is the most productive region of the Small Magellanic Cloud in terms of star formation but also the least studied one. In this paper, we investigate the star formation history of two fields located in the SW and in the NE portion of the Bar using two independent and well-tested procedures applied to the color–magnitude diagrams of their stellar populations resolved by means of deep *Hubble Space Telescope* photometry. We find that the Bar experienced a negligible star formation activity in the first few Gyr, followed by a dramatic enhancement from 6 to 4 Gyr ago and a nearly constant activity since then. The two examined fields differ both in the rate of star formation and in the ratio of recent over past activity, but share the very low level of initial activity and its sudden increase around 5 Gyr ago. The striking similarity between the timing of the enhancement and the timing of the major episode in the Large Magellanic Cloud is suggestive of a close encounter triggering star formation.

*Key words:* galaxies: evolution – galaxies: formation – galaxies: individual (Small Magellanic Cloud) – galaxies: interactions – galaxies: photometry – galaxies: star formation – galaxies: stellar content – galaxies: structure – stars: massive

*Online-only material:* color figures

## 1. INTRODUCTION

The Small Magellanic Cloud (SMC) is a fundamental laboratory to study the evolution of dwarf irregular galaxies (dIrr's). The SMC is the closest member of this class of systems, has a current metallicity ($Z \simeq 0.004$ as derived from H II regions and young stars) similar to that of the majority of dIrr's and a mass (between 1 and $5 \times 10^9\ M_\odot$, e.g., Kallivayalil et al. 2006 and references therein) at the upper limit of their range. Moreover, the SMC is a member of a triple system, a circumstance that favors studying the modulation of the star formation activities driven by interactions.

In order to derive the detailed, spatially resolved star formation history (SFH) of the SMC, we have started an international long-term project to study the evolution of the SMC in space and time (see Tosi et al. 2008). Our strategy is to achieve high photometric depth and spectroscopic resolving power over a large field of view by combining data sets from the ground and space. We are using the *Hubble Space Telescope* (*HST*), the Very Large Telescope (VLT), and the VLT Survey Telescope (VST) to observe a large sample of field stars and clusters across the SMC. These data will allow us to constrain the global SFH as well as the existence of chemical and age gradients.

For the cluster analysis, we have already presented deep photometry with *HST*'s Advanced Camera for Surveys (ACS) of seven intermediate-age and old populous clusters (Glatt et al. 2008a, 2008b, 2009, 2011). In combination with our VLT data, we find a complex age–metallicity relation for these clusters with a considerable spread in metallicity at any given age (see, e.g., Glatt et al. 2008b).

Concerning the SMC field analysis, our plan is to have color–magnitude diagrams (CMDs) several magnitudes fainter than the oldest main-sequence (MS) turnoff (TO) for the entire galaxy. To this purpose, we have observed six fields with the ACS (Sabbi et al. 2009), sampling regions characterized by different stellar and gas densities in the SMC Bar, in the Wing in the direction of the Large Magellanic Cloud (LMC), and in the outskirts (see Figure 1). A preliminary SFH analysis of such fields has been presented in Sabbi et al. (2009). We also have an ongoing Guaranteed Time Observation program at the VST (Ripepi et al. 2006) designed to cover with deep photometry the whole SMC and the Bridge connecting it to the LMC. These CMDs will allow us to infer for the first time the SFH of the whole SMC over the entire Hubble time, covering a much larger area with considerably better image quality than Zaritsky et al.'s (2002) data. We will derive the SFHs from the CMDs using the synthetic CMD technique (see, e.g., Tolstoy et al. 2009; Cignoni & Tosi 2010 and references therein).

SFHs of some SMC fields have been derived and presented by other authors, based on ground-based observations or *HST* studies of small individual regions (see Figure 1). Harris & Zaritsky (2004) derived the SFH of the SMC over $4^\circ \times 4\overset{\circ}{.}5$ to a depth of $V \lesssim 21$ using the Magellanic Cloud Photometric Survey (MCPS) UBVI catalog of Zaritsky et al. (2002). This is currently the most spatially extended study of the galaxy, but does not reach the oldest MSTO. The most comprehensive study of the old population of the SMC to date was carried out by Haschke et al. (2012) using RR Lyrae stars from the Optical Gravitational Lensing Experiment (Udalski et al. 2008). They find a uniform metallicity distribution across the SMC with a spread of more than 1 dex in [Fe/H]. Dolphin et al. (2001) analyzed the stellar content of the SMC halo, in a region close to the globular cluster NGC 121, using both *HST* Wide Field Planetary Camera 2 (WFPC2) and ground-based data.

* Based on observations with the NASA/ESA *Hubble Space Telescope*, obtained at the Space Telescope Science Institute, which is operated by AURA, Inc., under NASA contract NAS 5-26555. These observations are associated with program GO-10396.

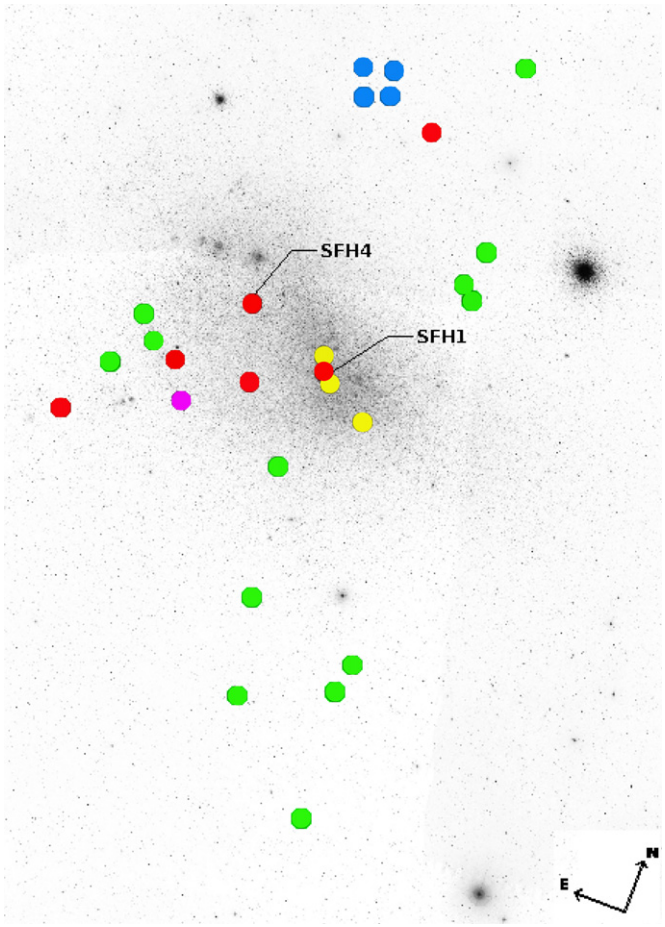


**Figure 1.** Spatial distribution of the six observed fields (red symbols) together with the observations from Dolphin et al. (2001) (blue symbols), McCumber et al. (2005) (magenta symbol), Noël et al. (2007) (green symbols), and Chiosi & Vallenari (2007) (yellow symbols), superimposed on the DSS image of the SMC.

(A color version of this figure is available in the online journal.)

Again with WFPC2, McCumber et al. (2005) studied the stellar content of a small portion of the SMC Wing. Chiosi & Vallenari (2007) derived the SFH in the vicinity of a few SMC clusters. Finally, Noël et al. (2007) and Noël et al. (2009) presented a deep ground-based study of 12 fields of the SMC, avoiding the densest regions, because of their high crowding conditions.

In this paper, we present the SFH of SFH1 and SFH4, the two most central fields of the six SMC regions we observed with *HST*/ACS (Sabbi et al. 2009). The apparent distances from the SMC optical center are about 24′ and 1° 52′, respectively. SFH1 is located in the SW portion of the SMC Bar, where the stellar density, gas, and dust contents are highest, while SFH4 is located to the NE of the SMC center, at 24′ south of NGC 346, the most active star-forming region in the SMC.

For a better assessment of the intrinsic theoretical uncertainties, the SFH is derived using two completely independent procedures for the application of the synthetic CMD method. We compare the two methods here and discuss the corresponding results. The other ACS fields observed by us and described by Sabbi et al. (2009) are being treated in the same way, and their SFH will be presented in a forthcoming paper.

We briefly describe our data in Section 2. The two procedures for the SFH derivation are summarized in Section 3, together with the results of their application to SFH1 and SFH4. Similarities and differences between the resulting SFHs are discussed in Section 4, while in Section 5 we compare our findings with previous literature. Concluding remarks follow in Section 6.

## 2. PHOTOMETRY AND CMDs OF SFH1 AND SFH4

The data for our six SMC fields were acquired with the ACS Wide Field Channel between 2005 November and 2006 January (GO-10396; P.I. Gallagher) with the F555W and F814W filters. The data reduction was performed with the program img2xym_WFC.09x10 (Anderson & King 2006), and the resulting magnitudes were calibrated in the Vegamag photometric system using Sirianni et al. (2005) recipes. For the sake of simplicity, from now on we will refer to the $m_{F555W}$ and $m_{F814W}$ magnitudes calibrated in the Vegamag system as V and I, respectively.

Extensive artificial star experiments were performed to test the level of completeness and the photometric errors of the data. They followed the approach described in Anderson et al. (2008), and the artificial stars were searched for with exactly the same procedure adopted for the real stars. We considered an artificial star as recovered if its input and output positions agree to within 0.5 pixels and the fluxes agree to within 0.75 mag. As done in the photometric analysis, we also required that each star was found in at least three exposures with a positional error <0.1 pixels per filter.

Details on both the data reduction and the artificial star tests can be found in Sabbi et al. (2009).

The final SFH1 and SFH4 catalogs contain about 29,200 and 17,300 stars, respectively, and the corresponding CMDs are shown in Figure 2, where the photometric errors are also plotted.[7] These CMDs reach almost 4 mag fainter than the oldest MSTO, thus allowing us to study the evolution of the regions over the whole Hubble time. The sub-giant branch (SGB) is well populated and its brightness extension, much larger than the photometric error at that magnitude level, suggests a prolonged star formation between 3 and 12 Gyr ago. The red giant branch (RGB) and the red clump (RC) also are well populated. In addition to these intermediate-age and old components, both CMDs show an MS blue plume and a blue loop (BL) sequence typical of late-type dwarf galaxies, corresponding to young high- and intermediate-mass stars.

Finally, the CMDs do not show any significant population of stars on the right of the lower MS, the CMD locus occupied by pre-main sequence (PMS) stars. This, in turn, suggests a negligible activity in the last 50 Myr (the average time spent by a solar-like star in PMS; see, e.g., Cignoni et al. 2010) compared to more active regions of the SMC-like NGC 346 or NGC 602 (see, e.g., Nota et al. 2006; Cignoni et al. 2009, 2011; Carlson et al. 2011).

## 3. SFH DERIVATION: THE TWO SYNTHETIC CMD APPROACHES

The SFH of SFH1 and SFH4 has been derived with the synthetic CMD method. As recently reviewed by Tolstoy et al. (2009) and Cignoni & Tosi (2010), this approach was first applied to nearby resolved galaxies 20 years ago (Tosi et al. 1991) and is now recognized as a powerful tool to disentangle the complex history of resolved galaxies. To both fields, we have applied it following two independent procedures: Cole's

[7] To be conservative, the plotted error bars correspond at each magnitude level to the larger value of the error resulting from the photometric package and from the artificial star tests.

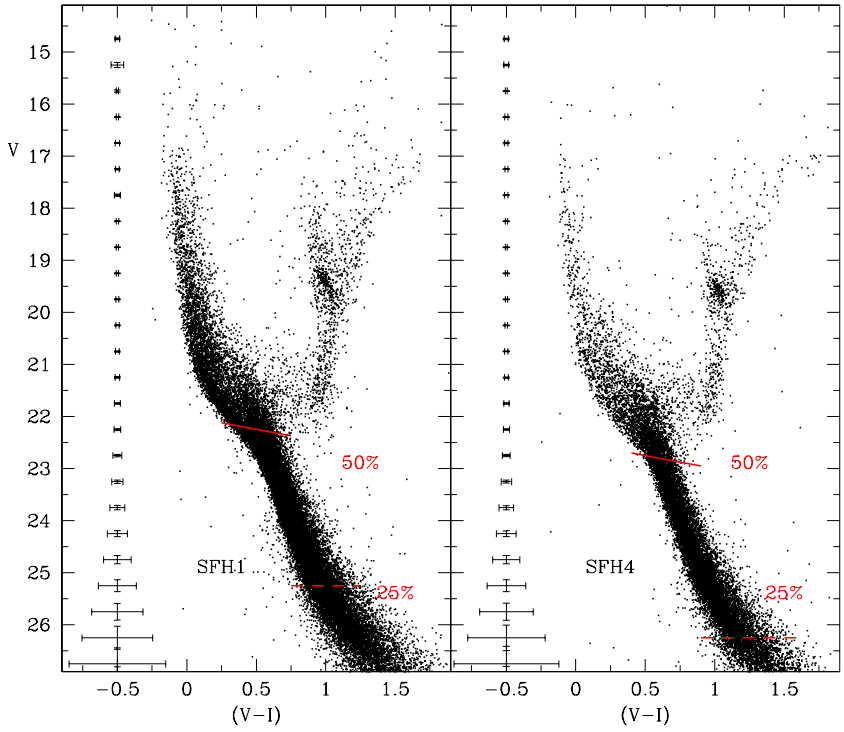


**Figure 2.** CMDs of the SFH1 (left panel) and SFH4 (right panel) field observed with the ACS/WFC. The solid and the dashed red lines indicate the 50% and 25% levels of completeness, respectively. Formal errors on the estimated photometry are shown on the left side of each CMD (see the text for details).
(A color version of this figure is available in the online journal.)

(e.g., Cole et al. 2007) and a combination of Cignoni's (e.g., Cignoni et al. 2006) and the Bologna (e.g., Tosi et al. 1991; Greggio et al. 1998; Angeretti et al. 2005) codes. These techniques supersede the classical isochrone fitting approach, allowing us to explore a much wider parameter space and to incorporate statistical and observational uncertainties. Nonetheless, their use is limited by the reliability of the adopted stellar tracks and color transformations, as well as the nature of the initial mass function (IMF; e.g., Section 4.1) and quality of the data. The recovered history is the best of all possibilities, but this does not necessarily imply that it is the actual solution nor that it is unique.

The procedures used here have already been tested in comparisons with each other and similar methods. Both groups participated in the Coimbra experiment in 2001 (see Skillman & Gallart 2002 and references therein), Cignoni's method has been applied to the derivation of the solar neighborhood SFH (Cignoni et al. 2006; Cignoni 2006) and in combination with the Bologna code to the analysis of the SMC young clusters NGC 346 (Cignoni et al. 2010, 2011) and NGC 602 (Cignoni et al. 2009), Cole's method has been compared with two different codes in the analysis of the dwarf irregular IC 1613 (Skillman et al. 2003) and the Cetus dwarf spheroidal (Monelli et al. 2010). Since the procedures are in continuous evolution, to improve both the reliability of the results and the efficiency of the computations, it is useful to perform further comparisons on deep and tight CMDs such as those of SFH1 and SFH4.

In the following, we briefly summarize commonalities and differences of the two methods. In both cases, the synthetic CMDs have been built using the results of the artificial star tests mentioned above to assign photometric errors and incompleteness to the synthetic stars.

### *3.1. Bologna Procedure*

The Bologna approach involves the comparison of the observed CMD with a library of synthetic CMDs computed with different values of metallicity, IMF, binary fraction, distance modulus, and reddening. Models have been calculated with the latest Padova stellar models (Bertelli et al. 2008, 2009) for masses between the hydrogen-burning limit and 20 $M_{\odot}$. Theoretical temperature and luminosity are transformed to the observational plane by means of the relations obtained by Origlia & Leitherer (2000) for the *HST* Vegamag photometric system. The synthetic CMD is created following a classical Monte Carlo procedure: (1) stellar masses and ages are randomly extracted from a time-independent IMF and a star formation law, (2) the stellar tracks are interpolated deriving the absolute photometry for the synthetic population, and (3) corrections for the distance modulus and the foreground reddening are applied. Then, the synthetic CMD is degraded to match both the completeness profile and the photometric error properties as derived from extensive artificial star tests (Sabbi et al. 2009). To be conservative, we have limited our fitting procedure to stars brighter than $V = 23$, whose completeness is better than 40% and photometric errors smaller than 0.05 mag.

The full SFH of a galaxy can be a complex function of time. To make the problem manageable, we were forced to limit the range of parameter space that our models cover on the basis of previous results and indications from our data. In order to reduce the computational time, the star formation rate (SFR) is parameterized as a set of constant values over adjacent temporal steps: a generic CMD is a linear combination of chosen basis CMDs, where each basis is a Monte Carlo extraction from a step star formation episode. The duration of each step is chosen in relation to the evolutionary timescale of the average stellar

mass of the step, ranging from 50 Myr (approximately the MS timescale for an 8 $M_{\odot}$ star) to 1 Gyr (as representative of the theoretical precision at 10 Gyr, i.e., 10%) for ages above 3 Gyr. The SFR is constant within each step. In this work, we deal with 90 basis CMDs, each representing the synthetic photometry of one of 18 age bins and one of five metallicities ($Z = 0.008$, $Z = 0.004$, $Z = 0.002$, $Z = 0.001$, $Z = 0.0004$). In order to reduce the Poisson fluctuations, all partial CMDs are generated with more than $10^6$ solar masses.

Within the framework of the adopted stellar tracks and atmosphere models, the most likely solution to the underlying SFH is the one which minimizes the differences between data and synthetic star counts over strategic regions of the CMD. The degree of likelihood is assessed through a $\chi^2$ function of the residuals. Our experience suggests that the performance of such minimization is very sensitive to the adopted CMD binning scheme. Both fine and coarse grids offer advantages as well as disadvantages (see, e.g., Cignoni et al. 2006). Along the MS, a fine grid is mandatory to study the old stellar generations, since they are tightly packed together in the CMD. However, such a solution would pay the penalty of underweighting the star counts along the upper MS which is Poisson dominated. Vice versa, a coarse grid would be more adequate to map the recent activity, but it would allow a worse resolution at early times. The situation is even worse with the evolved stars, where the theoretical uncertainties are typically larger than for MS stars: the CMD position of horizontal branch (HB) and RC stars is affected by a complex interplay of age, metallicity, mass loss, and helium content (see, e.g., Castellani et al. 2000); not only the color, but also the shape of the RGB are strongly affected by the color transformations from the theoretical to the observational plane and by the mixing length parameter (in a way which depends on the used wavelength). The BL morphology is affected by the He-burning cross sections (especially the $^{12}C(\alpha,\gamma)^{16}O$) as well as by the efficiencies of external convection, overshooting, and mass loss. Nevertheless, the study of evolved stars can prevent the ambiguities in models restricted to MS star counts, for example, when photometric errors and incompleteness hinder the possibility to trace the old activity by means of low-mass MS stars. Given these issues, the problem of the grid choice can be solved only by using a variable grid spacing. Several tests were conducted for finding the optimal configuration. Figure 3 shows our best scheme. To capture all the information contained along the MS, the grid spacing shrinks with luminosity, balancing the longer evolutionary times of lower mass stars and, at the same time, providing sufficiently good statistics in the upper MS. Toward the red part of the CMD the average grid spacing is coarser: this helps to take the uncertainties into account, while preserving the number of stars in specific phases.

Finally, the $\chi^2$ is minimized by means of a downhill simplex algorithm. In order to avoid local minima, the simplex is re-started from thousands of initial random positions. A bootstrap method is used to assess the effect of random errors. The search of the best SFH is repeated for each bootstrapped data set, producing a distribution of best solutions. The error bars on the final SFH represent one standard deviation using 100 bootstraps.

With this procedure, we have analyzed the CMD of SFH1 and SFH4. As a first step, we have derived the SFH assuming a two-exponent power-law IMF (see Kroupa 2001) with exponent $s = 2.3$, close to Salpeter's 1955[8] for masses above 0.6 $M_{\odot}$

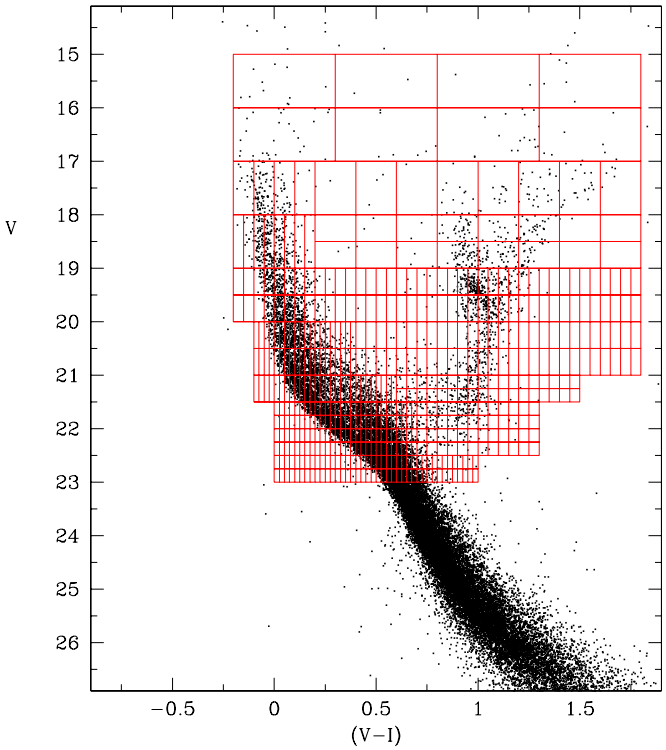


**Figure 3.** CMD grid used to derive the SFH via the Bologna procedure.
(A color version of this figure is available in the online journal.)

and $s = 1.3$ below, and a binary fraction (with primary and secondary mass extracted from the same IMF) of 30% (this parameter has no substantial impact on the fit quality). To reduce the parameter space, only three metallicities, $Z = 0.004$, $Z = 0.002$, and $Z = 0.001$, have been adopted. The distance modulus and the foreground reddening were allowed to vary freely. The solutions with the lowest reduced $\chi^2$ are listed as SFH1-A and SFH4-A for the respective fields.

In order to test how much the details of the solution depend on the allowed metallicity range, we calculated a second solution where the Padova tracks with $Z = 0.0004$ and $Z = 0.008$ were also included. These solutions are presented as SFH1-B and SFH4-B. These are generally consistent with the solutions obtained with the restricted metallicity range but provide a somewhat better match to the observed CMD as described in Section 4.1 below.

### 3.2. Simulated Annealing Procedure (Cole's Method)

The code developed by Cole has many features in common with the Bologna code, but also incorporates some differences in the treatment of the Hess diagram data and in the calculation of the merit function that measures the relative likelihood of various solutions. Because the errors in extracting detailed information from a CMD are dominated by systematic effects, the application of multiple fit procedures to the same data can provide important insight into which features of the SFH are robust and which may be artifacts.

Cole's SFH-fitting code begins with a set of theoretical isochrones interpolated to a fine grid of age and metallicity in order to create a synthetic CMD with no gaps. The most recent isochrones from the Padova models are used; all calculations are made in the *HST* Vegamag system to minimize the possibility of introducing errors in transformation equations. The synthetic CMDs are binned in age and metallicity ($Z$) to increase the speed

[8] Salpeter's IMF has exponent $s = 2.35$ and the form $\int_0^{+\infty} m\,\phi(m)\,dm = 1$ and $\phi(m) = m^{-s}$.

of computing and to avoid "overfitting" noise in the CMDs. We begin with bins that are evenly spaced by ≈0.10 in Δlog(age) and 0.20 in Δlog($Z$), and merge adjacent bins when the noise level of the solutions indicates there is insufficient information content in the CMD to resolve the fine age bins.

The CMD is divided into a regular grid of color–magnitude cells, and the expectation value of the number of stars in each cell for an SFR of 1 $M_{\odot}$ yr$^{-1}$ is calculated from the isochrones. There are several parameters that are taken as fixed constants during the solution. These include the IMF, fraction of binaries and mass ratio distribution function, and the distance modulus and reddening. The adopted IMF is from Chabrier (2003), and the binary fraction and mass ratios are parameterized based on Duquennoy & Mayor (1991) and Mazeh et al. (1992). In this prescription, 35% of stars are single and the rest are binary. The binaries are divided into "wide" and "close" binaries in a 3:1 ratio; the secondaries in the wide systems are drawn from the same IMF as the primaries, but in the close systems the secondary masses are drawn from a flat IMF. The distances and reddenings are initially constrained to the values given in Sabbi et al. (2009), but are varied if the resulting synthetic CMDs are mismatched to the data.

No age–metallicity relation is explicitly assumed, but a range of metallicities at each age is allowed, constrained by the color range of the data. In some cases, there is little leverage in the CMD to constrain the metallicity, so outside information is used to choose the metallicity. For example, the $V - I$ color of the upper MS is not strongly metallicity dependent, so we adopt a metallicity of $Z = 0.004$ based on H II region and Cepheid metallicities for the youngest stellar populations in the SMC Bar. For stars with ages on the order of ≈1–7 × $10^8$ yr, this metallicity also gives a good match between the colors of the blue supergiant stars in SFH1 and the Padova models. For older ages, ranges of metallicity at each age are allowed.

A synthetic CMD is constructed by convolving the weighted, color–magnitude binned isochrones with the color and magnitude errors and incompleteness functions determined by artificial star tests. In the fit process, linear combinations of the individual synthetic CMDs are added to find the composite CMD that best matches the data. Because many cells in the Hess diagram are empty or contain few stars, a maximum likelihood test based on the Poisson distribution must be used instead of a $\chi^2$ statistic (Cash 1979). A direct search of parameter space is infeasible because there may be dozens of age and metallicity bins in the solution; additionally, effects such as age–metallicity degeneracy can easily produce a large number of false, local maxima in the likelihood space. Because of this, we use a simulated annealing approach, in which a simplex of initial guesses at the SFH is randomly perturbed and the changes are rejected with some probability if they worsen the fit. The SFRs are transformed according to an arcsin function prior to fitting in order to prevent negative SFRs from being considered.

Error bars on the SFH are calculated by testing each age–metallicity bin of the best-fit solution in turn. The SFR in the bin under consideration is forced away from the optimal solution and the fitting procedure is redone, with the tested bin held fixed. The 1$\sigma$ error on the SFR of the bin is taken to be the value beyond which no fit can be found that is within 1$\sigma$ of the global best fit. Because the total number of stars is fixed, a deficiency of stars in one age bin can often be partially compensated by increasing the SFR in nearby bins; this means that error bars are fairly large and the SFR in adjacent bins can be strongly anticorrelated. Because there are always unmodelled populations (including Galactic foregrounds, background galaxies, and simple bad data) and there may be poorly fit stellar sequences (e.g., the colors of RGB stars), the overall fit quality as measured by the equivalent of a $\chi^2$ statistic is usually found to be quite poor; only the relative likelihoods are of any meaning. The most likely SFH to match the observed CMD is driven by the most populous cells in the CMD; because these are frequently near the faint end of the data where incompleteness is high, it is absolutely essential to have a very accurate model of the incompleteness to obtain robust results.

The ACS data are of high quality, but incompleteness sets in at a relatively bright level. The large number of stars and low average error leads us to use magnitude bins 0.08 mag high and color bins 0.04 mag wide. In order to avoid systematics due to the incompleteness, we restricted the comparison to magnitudes $15 \leqslant I \leqslant 22$. Because there are significant uncertainties in modeling the colors of RGB and RC stars, we restricted our fits to the MS and SGB. We considered a set of isochrones binned by 0.10 in log(age) from 4 Myr ⩽ age ⩽ 13.5 Gyr ($6.60 \leqslant$ log(age) $\leqslant 10.13$); below log(age) = 8.60 the decreasing number of bright tracer stars led us to double the size of the age bins. We considered metallicities of $Z = 0.00015$, 0.0004, 0.0006, 0.001, 0.0015, 0.0024, and 0.004.

We begin with the distance moduli and reddenings from Sabbi et al. (2009), but found that these needed to be modified in order to obtain the best match to the data with the Padova isochrones. For SFH1, we found the best distance modulus $(m - M)_0 = 18.83$ and reddening $E(B - V) = 0.08$, while in SFH4 we used 18.85 and 0.12. In both fields, the values are within 1$\sigma$ of the initial guesses. In SFH1, we found that the model upper MS was significantly narrower and bluer than the data with the adopted reddening value, so we were forced to introduce an extra reddening component. We adopted the simple expedient that all populations younger than log(age) = 7.60 were subject to double the mean reddening of the field, while stars with $7.60 \leqslant$ log(age) $<$ 8.00 were assigned a reddening halfway between the younger and older stars. Differential reddening in the central SMC has previously been observed by Zaritsky et al. (2002), who used multicolor photometry to derive line-of-sight extinction corrections to individual bright SMC stars. They found a mean $A_V = 0.18$ mag for stars with 5500 K ⩽ $T_{\rm eff}$ ⩽ 6500 K, and $A_V = 0.46$ mag for stars with $T_{\rm eff} \geqslant$ 12,000 K; these numbers are in reasonable agreement with the values adopted here for SFH1. Zaritsky et al. (2002) discuss the physical reality of their derived reddening distributions and conclude that small-scale reddening variations may reasonably be attributed to residual gas and dust in star-forming regions. The vast majority of old, cool stars will not be seen through star-forming regions, and so the small highly reddened tail of the old population will not strongly influence the mean reddening. Because the amount of differential reddening has high spatial frequency, the numerical agreement (as in SFH1) or lack thereof (as in SFH4) with the conclusions of Zaritsky et al. (2002) must be considered fortuitous.

Cole's best-fit solutions are presented here as SFH1-C and SFH4-C, respectively, for the two fields.

## 4. RESULTS: SFH OF TWO FIELDS IN THE SMC BAR

The properties of the three SFH solutions for each field are summarized in Table 1. While the two procedures use the same photometry and isochrones, they differ in a number of important respects. The application of two completely independent codes

**Table 1**
Summary of SFH Solution Parameters[a]

| Solution | Method | $(m-M)_0$ (mag) | $E(B-V)$ (mag) | IMF | CMD Binning (color×mag) | Metallicities ($Z \times 10^3$) |
|---|---|---|---|---|---|---|
| Field SFH1 | | | | | | |
| SFH1-A | Bologna | 18.77 | 0.11 | Kroupa (2001) | Variable[b] | 1, 2, 4 |
| SFH1-B | Bologna | | | | | 0.4, 1, 2, 4, 8 |
| SFH1-C | Cole | 18.83 | 0.08[c] | Chabrier (2003) | 0.04 × 0.08 | 0.15, 0.4, 0.6, 1.0, 1.5, 2.4, 4.0 |
| Field SFH4 | | | | | | |
| SFH4-A | Bologna | 18.80 | 0.11 | Kroupa (2001) | Variable[b] | 1, 2, 4 |
| SFH4-B | Bologna | | | | | 0.4, 1, 2, 4, 8 |
| SFH4-C | Cole | 18.85 | 0.12 | Chabrier (2003) | 0.04 × 0.08 | 0.15, 0.4, 0.6, 1.0, 1.5, 2.4, 4.0 |

**Notes.**
[a] All models based on the Padova isochrone set; see the text for details.
[b] See Figure 3.
[c] Differential reddening assumed for stars younger than 100 Myr.

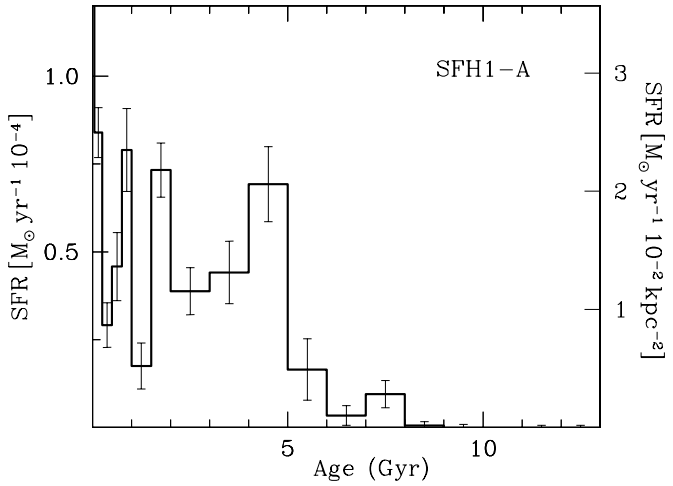


**Figure 4.** SFH for the SFH1 field, obtained with a restricted metallicity range (solution SFH1-A). The star formation rate is given both in $M_\odot$ yr$^{-1}$ (left ordinate) and per unit area ($M_\odot$ yr$^{-1}$ kpc$^{-2}$, in the right ordinate).

to derive the SFH allows us to identify the most model-independent features of the SFH, gives insight into the areas of the CMD that are driving the fitting procedures to the results they give, and gives an estimate of the systematic uncertainties in the fits.

### 4.1. SFH1 Field

The SFH1-A (restricted metallicity) solution which gives the lowest (2.6) reduced $\chi^2$ is shown in Figure 4 (error bars represent $1\sigma$ uncertainty), while the corresponding synthetic CMD is shown in the middle panel of Figure 5. The left panel of the same figure shows the observational CMD for a direct comparison. Our best distance modulus and reddening are $(m-M)_0 = 18.77$ and $E(B-V) = 0.11$, respectively. According to this solution, the SFR has been extremely low during the earliest 6–7 Gyr, with a strong and rapid increase around 5 Gyr ago. From then on, the star formation activity has been typically gasping, with ups and downs with respect to an average almost constant rate.

In the middle row of Figure 6, we plot the luminosity function (LF) of blue and red stars (first and second column from the left, respectively) in the observed CMD and in the one resulting from SFH1-A. The top and bottom panels show for comparison the result when the SFH is searched using IMF exponents $s = 2.0$ and 2.5, respectively, for stars above 0.6 $M_\odot$.

Despite a somewhat high reduced $\chi^2$ 2.6, this model is successful in describing the main features of the data.

However, when the results are examined in detail, a few noticeable issues can be identified. First of all, the synthetic upper MS is sharper than the observational one. As already noted by Sabbi et al. (2009), such a broadening may indicate an additional absorption. One explanation could be that the SFH1 field is in the main body of the SMC and the reddening material may be patchy and cover not uniformly all lines of sight. Indeed, this is what is observed in the extensive analysis of Haschke et al. (2011), who suggests for SFH1 a broader reddening distribution[9] ($\sigma_{E(V-I)} \approx 0.12$ mag) with respect to SFH4 ($\sigma_{E(V-I)} \approx 0.09$ mag). Yet other possibilities are that a fraction of massive MS stars is affected by rotation, which can lead to widened upper MSs in young clusters (see, e.g., Grebel et al. 1996), or a different SMC depth along SFH1 and SFH4's lines of sight.

Our model slightly but systematically underestimates the number of blue massive stars brighter than $V \approx 19$ by 20%–30% (see the middle panel of the first column in Figure 6). A flatter IMF could mitigate such discrepancy (see the top panel of the first column in Figure 6), but the corresponding model would underestimate the number of low-mass stars (see the discrepancy between $V = 24$ and $V = 26$ in the top panel of the second column in Figure 6).

As far as the evolved stars are concerned, the synthetic CMD matches well both the SGB magnitude spread (that is a signature of the age spread) and the RGB color dispersion below the RC luminosity. However, there are several differences as well: (1) the predicted RC morphology is irregularly shaped, while the observational RC is smooth and rather elliptical. This difference may be partially explained by the coarse metallicity resolution of our model, but also by a small amount of differential reddening; (2) the synthetic CMD overestimates the number of RC stars by about a factor of two; a steeper IMF could slightly mitigate this mismatch (see the bottom panel of the second column in Figure 6), but at the expenses of the upper MS fit; and (3) the RGB stars brighter than the RC are too blue (even if the predicted counts match exactly the observed ones). This suggests that our models are too metal poor or, more likely, that the adopted color transformations systematically fail near the RGB tip.

[9] Reddening values from the red clump method are available through the German Astrophysical Virtual Observatory interface at http://dc.zah.uni-heidelberg.de/mcx.

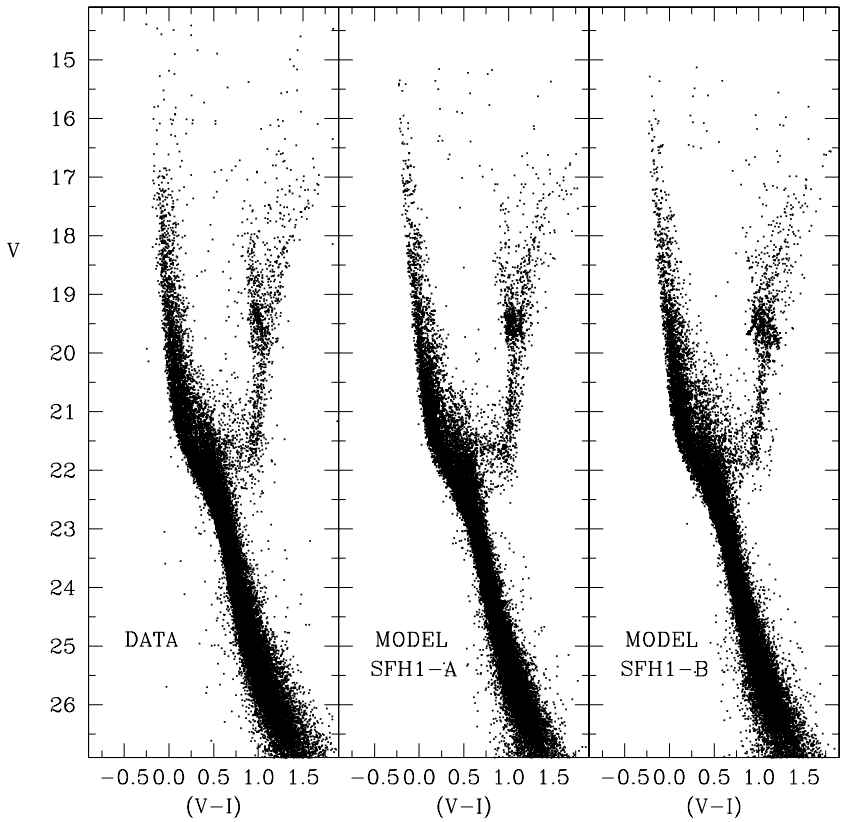


**Figure 5.** Synthetic CMD for the solution SFH1-A (middle panel) and SFH1-B (right panel) compared with the observational CMD (left panel).

We investigate the effect of metallicity on the SFH found via the Bologna procedure by adding the Padova tracks with $Z = 0.008$ and $Z = 0.0004$ (solution SFH1-B). The top left panel of Figure 7 shows the resulting SFH, while the other panels of the same figure present the mass fraction contributed by each metallicity.

Overall, the solutions SFH1-A and SFH1-B are rather similar (see Figure 8), both being characterized by a long quiet period at the oldest epochs. However, solution SFH1-B shows some different features. First, the early activity is slightly higher, a direct consequence of the lower initial metallicity; then, the activity between 0.5 and 3 Gyr ago is smoother than in SFH1-A.

We find with additional test models that the epoch of the first peak of star formation activity is progressively earlier for decreasing values of the adopted lowest metallicity. We are thus confident that our conclusion of a long almost quiescent period earlier than 5 Gyr ago is robust, although we do see and predict some stars as old as 10–12 Gyr.

Concerning the recovered chemical history, we find that the largest stellar mass fraction is produced at $Z = 0.001$, while the contribution from $Z = 0.004$ is only a few percent. Generally, the metallicity increases with time.

From the point of view of the fit quality, the new solution improves the CMD match, yielding a reduced $\chi^2$ of about 2.3. The differences are visible both in the synthetic CMD of Figure 5 (right panel) and in the LF (third and fourth columns) of Figure 6. Model SFH1-B reproduces the upper MS star counts and morphology better than model SFH1-A (compare the middle panel of the third column with the middle panel of the first column in Figure 6), but some problems still affect the simulation: (1) the synthetic CMD shows a hint of a red HB, which is not observed in the data; (2) the number of BL stars is still underpredicted; (3) the RGB above the RC is too blue; and (4) the predicted RC is still overpopulated and irregularly shaped.

Given these results, especially the improvement along the upper MS, model SFH1-B is globally better than SFH1-A, even if neither of them is fully satisfactory.

The result of applying Cole's CMD-fitting procedure to SFH1 is shown in Figure 9. The left panel shows the data, binned $0.04 \times 0.08$ in $(m_V - m_I, m_I)$, while the middle and the right panels show the best-fit synthetic CMD (SFH1-C) and map of residuals, respectively. The fit procedure has matched the LF and mean color of the stellar sequences well in general. The data and the model can be readily distinguished from one another because the data are just one instance of a random draw from the parent population and contain unmodelled noise, while the model represents the best guess at the pure parent population and is therefore more smoothly distributed.

Among the well-matched features are the color and vertical extent of the RC and its upward extension to $I \approx 17$, the enhancement in the SGB at $I \approx 20.8$, and the nearly vertical finger of stars at $V - I \approx 0.5$ corresponding to an intermediate-age MSTO. Notable areas of mismatch include the failure to reproduce the width of the MS (most obvious for $I \lesssim 21$), and the factor of two overproduction of RC stars ($I \approx 18.5$, $V - I \approx 1$). There is a sparsely populated red HB in the model that is not apparent in the data; this may be related to the general factor of two overproduction of low-mass core helium-burning stars, to poor constraints on the detailed element abundances at ancient times, and/or to gaps in modeling the physics of HB envelopes.

The SFH over the period from 0.5 to 13.5 Gyr ago for SFH1-C is given in Figure 10. The SFH is characterized by

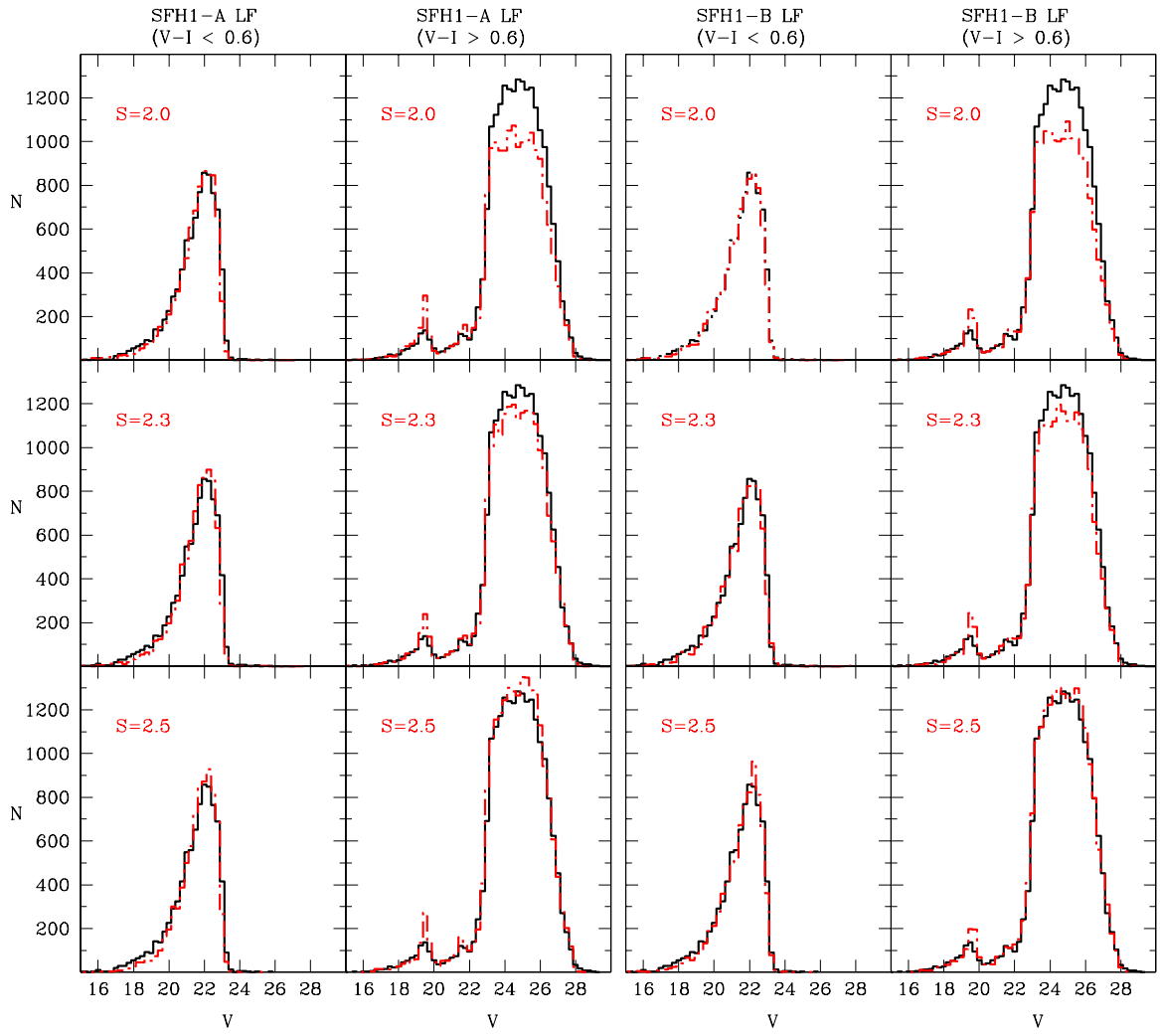


**Figure 6.** SFH1: predicted (red dot-dashed histograms) and observational (black solid histograms) LFs for stars bluer (first and third columns) and redder (second and fourth columns) than $V - I = 0.6$ for the model solutions SFH1-A (first two columns) and SFH1-B (third and fourth columns). Models in the top, middle, and bottom panels are computed with IMF exponents above 0.6 $M_{\odot}$ $s = 2.0$, 2.3, 2.5, respectively.

(A color version of this figure is available in the online journal.)

a very low SFR for several billion years before a rapid increase about 5 Gyr ago. This is the event that produces the features in the MS and SGB of the SFH1 CMD. The SFH remains at a similar elevated level after the 5 Gyr event, with some fluctuations.

Overall, the SFH of the SFH1 field, based on the synthetic CMDs from the Bologna and Cole procedures, is characterized by the following features.

1. The first 6–8 Gyr were rather quiescent and only a small fraction of the stars in this field was formed during these old epochs. The inferred average rate of star formation for ages older than ≈5 Gyr is only $\approx 3 \times 10^{-3}$ $M_{\odot}$ yr$^{-1}$ kpc$^{-2}$.
2. About 5–6 Gyr ago, SFH1 experienced a remarkable enhancement in the stellar production: over ≈1 Gyr the activity ramped up to about $2.2 \times 10^{-2}$ $M_{\odot}$ yr$^{-1}$ kpc$^{-2}$. The age and magnitude of this enhancement is robust to choices of IMF, CMD gridding, reddening, assumed metallicity, and details of the fitting procedure.
3. The average SFH has not dropped significantly from its peak at 5 Gyr ago, but the degree of burstiness in the solutions is model dependent. SFH1-B shows a relatively smooth recent history, while SFH1-C shows a factor of two drop in SFR between 3–4 Gyr ago with a subsequent recovery and SFH1-A shows repeated gasps from 0 to 2 Gyr ago. The reasons for this range of behavior are considered in Section 4.3 below.

It is worthwhile to quantify the stellar mass produced in each age interval (see the cumulative mass function in Figure 11). According to solution SFH1-B, the SFH1 field assembled a small fraction (11%) of its stellar mass before 6 Gyr ago, while a significant fraction (about 40%) was assembled only in the last 2 Gyr. For comparison, SFH1-C predicts that 17% of the stars were formed prior to 6 Gyr, and 33% over the past 2 Gyr.

### 4.2. SFH4 Field

The history of the SFH4 field was determined in similar fashion to the SFH1 field, using three sets of simulations (see Table 1). The recovered SFH for case SFH4-A is shown in Figure 12.

As in SFH1, the star formation proceeded at a low level until 5–6 Gyr ago, when it rose to almost the same amplitude of the first peak in SFH1. Afterward, the activity started a slow but steady decline until now, and only in the last 50 Myr it reached higher levels (mimicking in this respect the behavior of

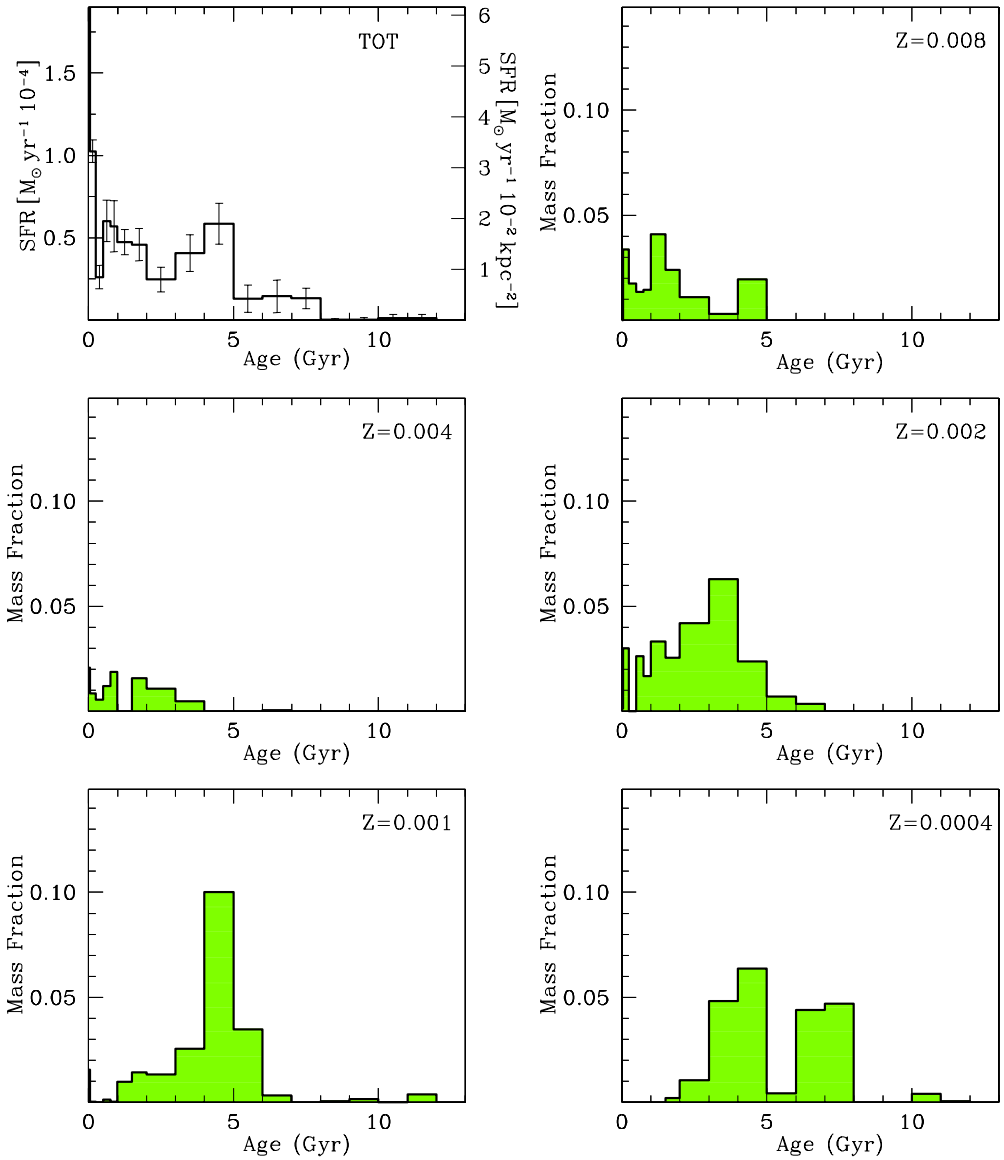


**Figure 7.** SFH for the SFH1 field resulting from models which include also the metallicities $Z = 0.008$ and $Z = 0.0004$ (solution SFH1-B). The top left panel shows the total SFH while the others display the contribution from each of the labeled metallicities.

(A color version of this figure is available in the online journal.)

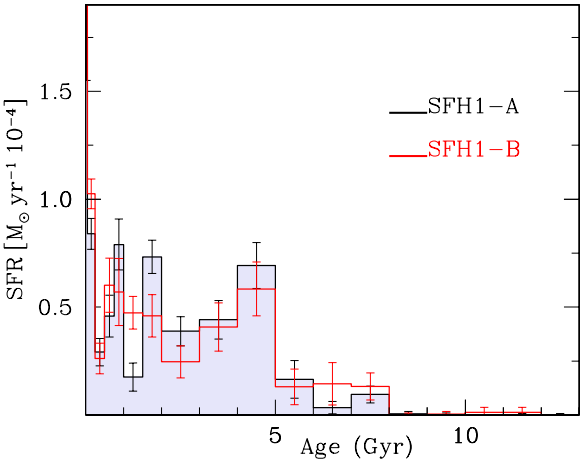


**Figure 8.** Recovered SFHs for SFH1 using the Bologna procedure: SFH1-A vs. SFH1-B. The latter is a better match to the data.

(A color version of this figure is available in the online journal.)

SFH1-A). Concerning distance and reddening, the recovered values ($(m - M)_0 = 18.80$ and $E(B - V) = 0.11$) are not significantly different from those obtained for SFH1. The corresponding reduced $\chi^2$, about 1.8, is significantly lower than the best value obtained for SFH1. Indeed, a visual inspection of the synthetic CMD (middle panel of Figure 13) confirms a very good agreement with the observational counterpart: our best model can reproduce the position and the morphology of the MS, the SGB and the RGB (above and below the RC). The only minor mismatches are in the BL region, which is underpopulated in our model, and in the SGB luminosity distribution, which is slightly more discontinuous than in the data.

As for SFH1, we expanded the metallicity range to include the values $Z = 0.008$ and $Z = 0.0004$ and re-derived the SFH. The essential features of the new solution (SFH4-B; see Figure 14) are not changed (see Figure 15 for a comparison SFH4-A vs SFH4-B): there is still a long quiet initial period, followed by a rapid enhancement of the activity and a subsequent decline. According to the solution SFH4-B, most of the stars ever formed in SFH4 have metallicities around $Z = 0.001$.

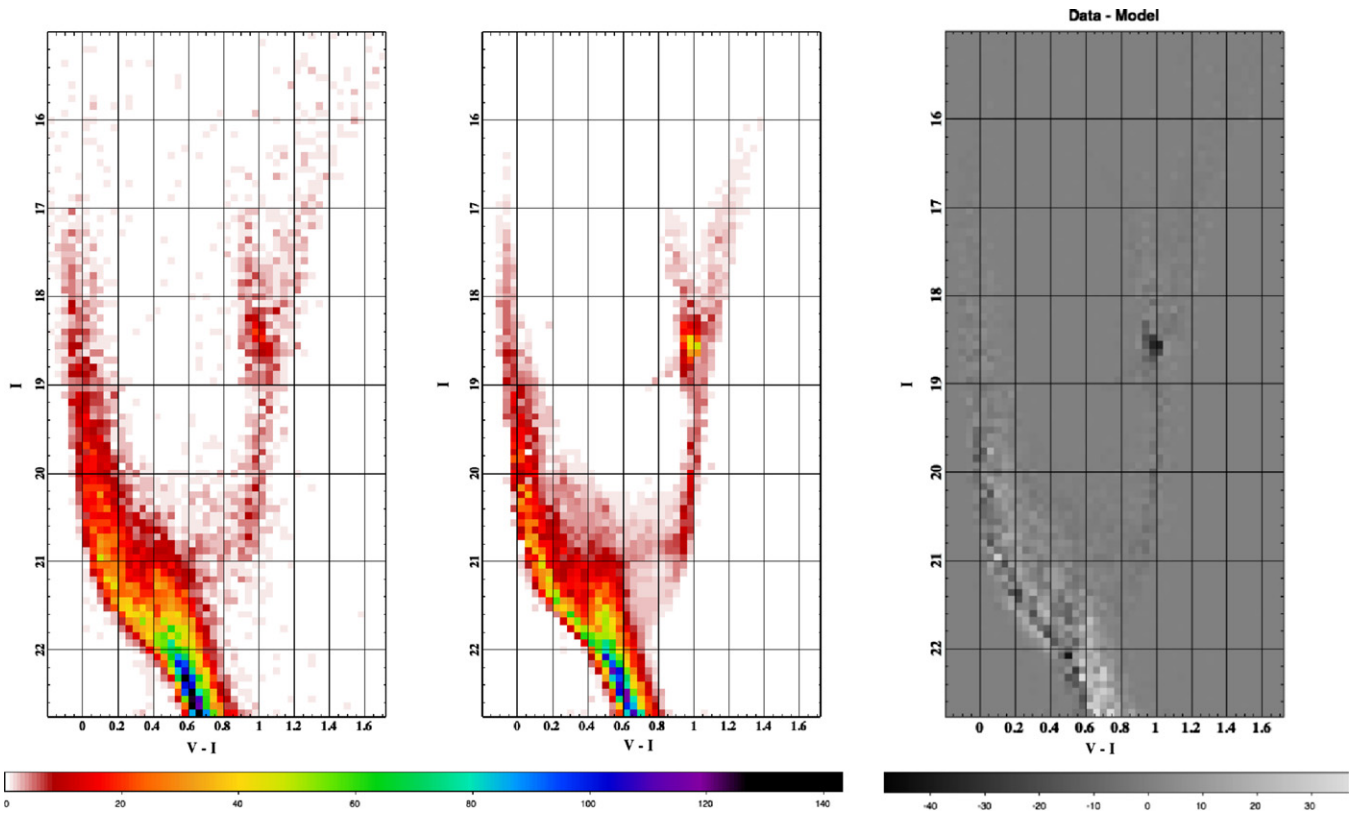


**Figure 9.** Left panel: observed Hess diagram for the SFH1 field of the SMC Bar, created by binning the data by 0.04 in color and 0.08 in magnitude; middle panel: synthetic CMD from the SFH1-C model (see the text for details); right panel: difference Hess diagram between the data and SFH1-C solution.

(A color version of this figure is available in the online journal.)

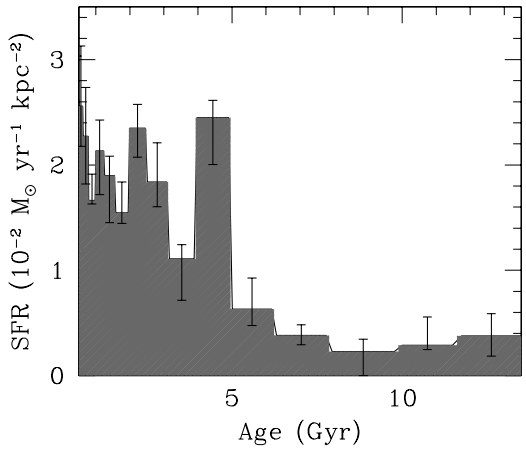


**Figure 10.** Long-term history of the SFH1 field from solution SFH1-C. Significant star formation commenced ≈5 Gyr ago and the rate has remained high, with some fluctuation, ever since.

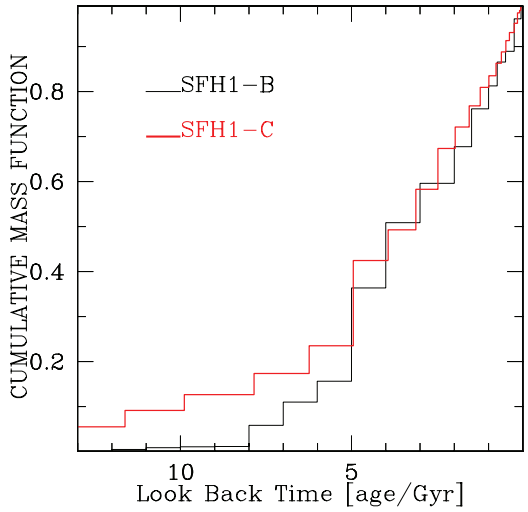


**Figure 11.** Cumulative mass function in SFH1 according to the solutions SFH1-B and SFH1-C.

(A color version of this figure is available in the online journal.)

In terms of fit quality, solution SFH4-B improves the match to the data significantly, leading to a reduced $\chi^2$ of about 1.3. The corresponding synthetic CMD is excellent (Figure 13, right panel) and the only detectable discrepancy is around the BL phase, still slightly underpopulated by the model. Unlike in SFH1, the number of RC stars is well matched (see the LF in the right panel of Figure 16). The fit to SFH4 using Cole's method shows similar results, with a better fit to the upper MS than in SFH1 because the observed sequence is narrower in color, and an overproduction of RC stars. The observed Hess diagram, synthetic diagram from solution SFH4-C, and the difference between the two are shown in Figure 17.

SFH4-C is broadly similar to SFH1-C, but the mean SFR is lower at all ages, commensurate with the smaller number of stars in the field (Figure 18). It is notable that the onset of significant star formation occurs simultaneously in the two fields, to within the ±1 Gyr precision of our data. However, the SFH4 field shows a decrease in SFR relative to SFH1 over the last ≈1.5 Gyr (which is obvious from a comparison of the RC morphology and upper MS LF of the two fields).

According to the solution SFH4-B (see the cumulative mass function of Figure 19), about 60% of the stellar mass has been

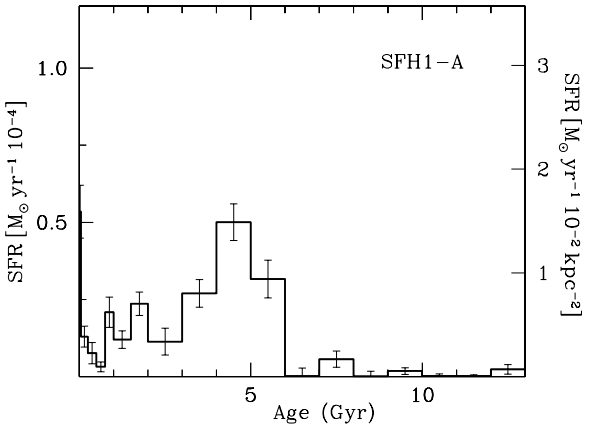


**Figure 12.** Best recovered SFH with restricted metallicity range (solution SFH4-A) for the field SFH4.

produced between 6 Gyr and 2 Gyr ago, which is higher than the fraction of mass (48%) produced in SFH1 in the same period. On the other hand, 16% of the total mass was already in place before 6 Gyr ago, which is comparable with the production in SFH1 (11%). The former difference is compensated in the last two Gyr, when SFH1 has turned into stars about twice the mass fraction of SFH4. While in the SFH1 field, the Bologna solution produced a younger result than the Cole solution, in SFH4 the situation is reversed. The solution SFH4-C predicts that only 7% of the stellar mass was in place before 6 Gyr ago, while 29% was astrated in the past 2 Gyr.

### *4.3. Comparison of the Two Methods*

We have derived the SFH of the field stars in the SMC Bar using two different synthetic CMD techniques. Figure 20 shows the results plotted together on the same scale to illustrate the similarities and differences. For SFH1, both SFHs indicate a major activity in the last 5 Gyr, an overall plateau (on average) since then on, and a spike in the last 50 Myr. The major differences concern: (1) the exact epochs of the peaks between 250 Myr and 4 Gyr ago (around 1.5 Gyr ago in Bologna's solution and 2.5 Gyr ago in Cole's solution); and (2) the rate in the period 8–13 Gyr ago, which is slightly stronger in Cole's solution.

The agreement for the field SFH4 is good as well: both models predict a star formation onset between 4 and 5 Gyr ago, followed by a slow decline and a very recent burst. The major difference here is the rate of decline in SFR after the 4–5 Gyr enhancement, with Cole's solution showing a constant activity for about 2.5 Gyr and Bologna's solution showing a faster decline followed by a mild enhancement around 1.5 Gyr ago.

In both fields, the only ages in which the SFRs differ by significantly more than the formal error bars on the solutions are in the period 1.5–3 Gyr ago, with Cole's solution showing consistently higher SFR. Part of this difference stems from the slightly higher SFR derived by Cole's method at all ages, owing to the different mean stellar masses resulting from the different assumed IMFs and binary fractions. The effect may be exacerbated in the 1.5–3 Gyr age range because of the interplay between age and the different metallicity values considered, and the fact that Cole's procedure does not consider the RC in calculating the best-fit SFH. Consideration of a very large number of metallicity values tends to produce smoother SFHs than those derived using only a few metallicities (e.g., Cole et al. 2009).

Concerning the distance modulus, Cole's best values (18.83 for SFH1 and 18.85 for SFH4) are slightly higher than Bologna's

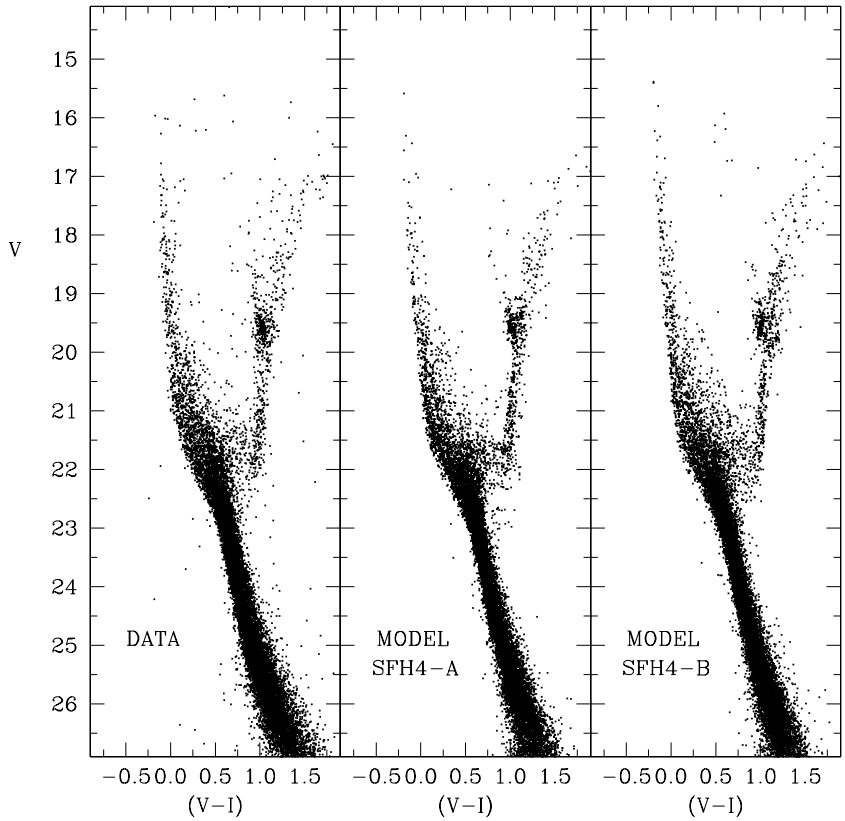


**Figure 13.** Synthetic CMD for the solution SFH4-A (middle panel) and SFH4-B (right panel) compared with the observational CMD (left panel).

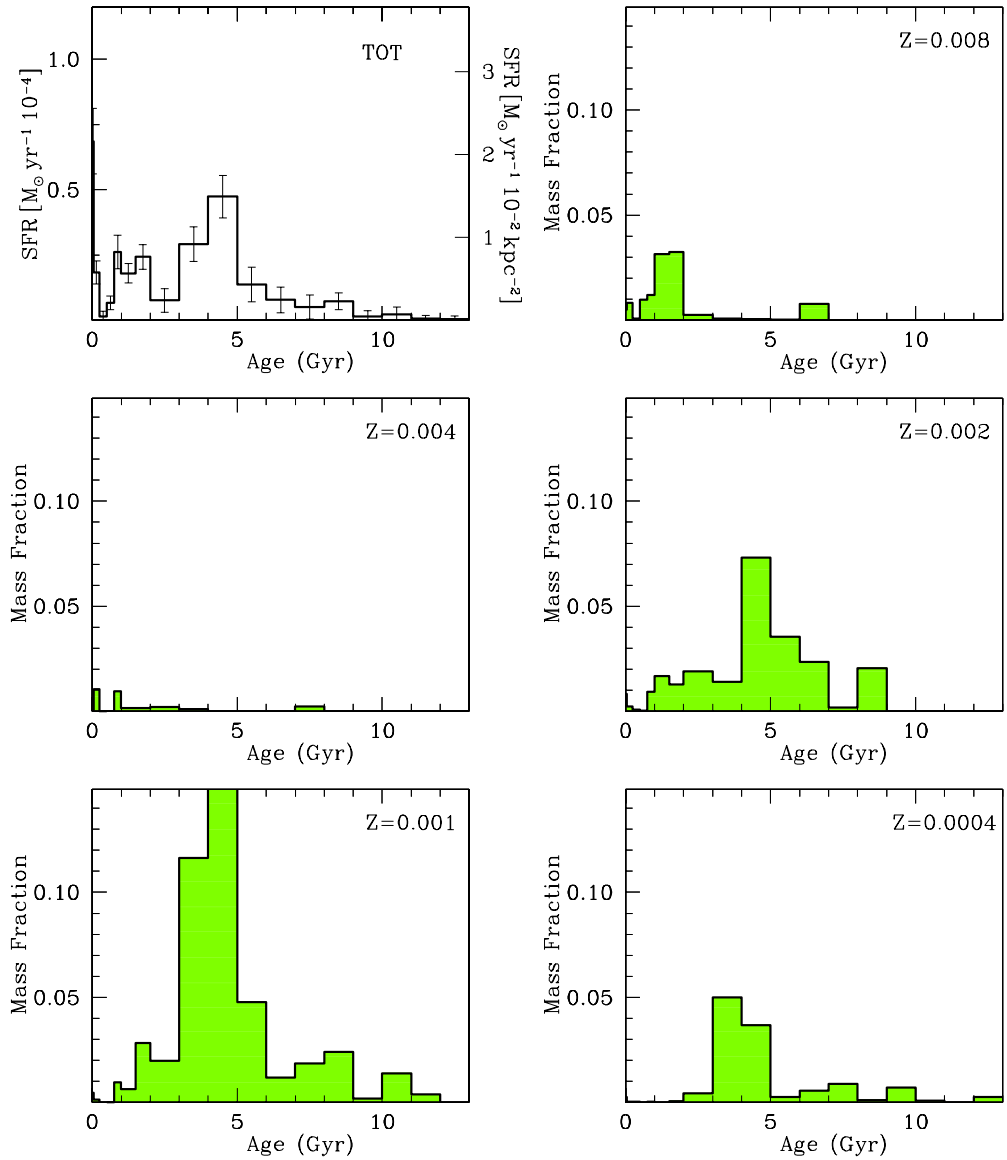


**Figure 14.** Best SFH (solution SFH4-B) resulting from models which include also the metallicities $Z = 0.008$ and $Z = 0.0004$. The top left panel shows the total SFH while the others display the contribution from each of the labeled metallicities.

(A color version of this figure is available in the online journal.)

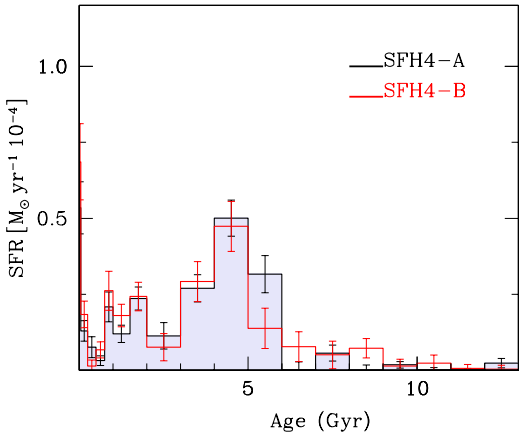


**Figure 15.** Comparison between the solutions SFH4-A and SFH4-B.

(A color version of this figure is available in the online journal.)

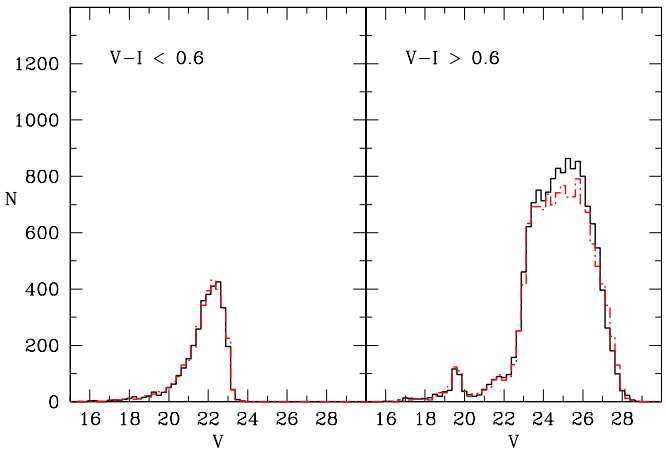


**Figure 16.** Predicted LF (red histograms) for the solution SFH4-B vs. the observed (black histograms) LF. The left-hand and the right-hand histograms are for stars bluer and redder than $V - I = 0.6$, respectively.

(A color version of this figure is available in the online journal.)

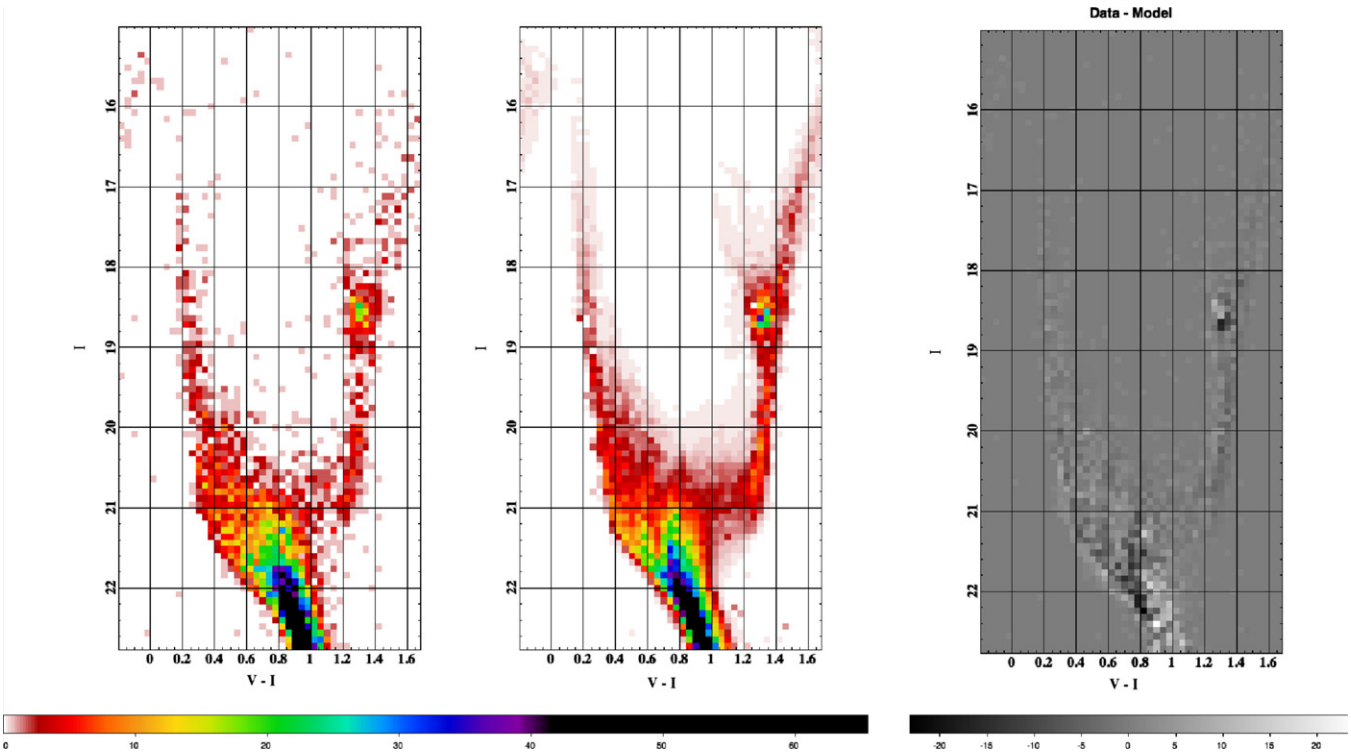


**Figure 17.** Left panel: observed Hess diagram for the SFH4 field; middle panel: synthetic Hess diagram from solution SFH4-C; right panel: difference between the two.

(A color version of this figure is available in the online journal.)

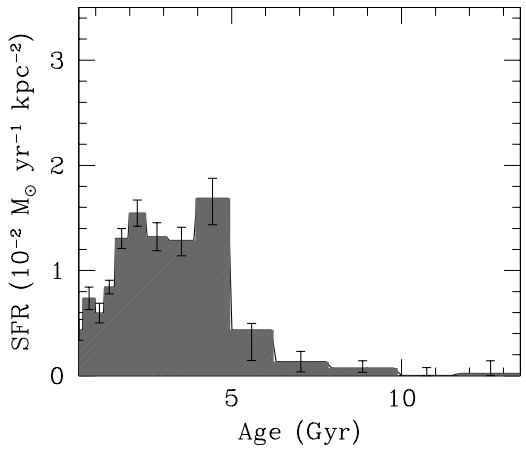


**Figure 18.** Long-term history of the SFH4 field from solution SFH4-C. Similar to SFH1, the field "switched on" ≈5 Gyr ago. The SFR has been declining over the past ≈1.5 Gyr in this locale.

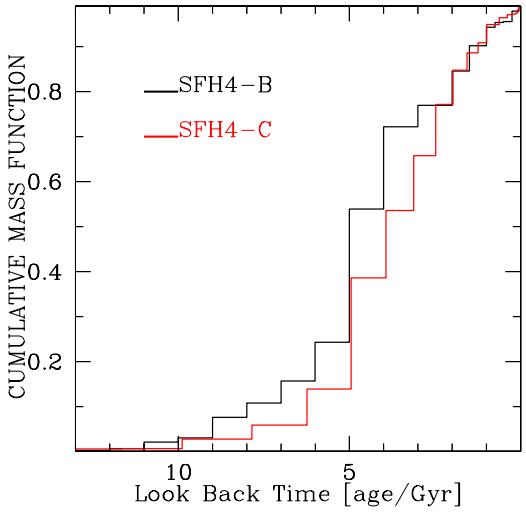


**Figure 19.** Cumulative mass function in SFH4 according to the solutions SFH4-B and SFH4-C.

(A color version of this figure is available in the online journal.)

(18.77 and 18.80). In SFH1, these offsets may be due to the higher reddening required by the Bologna method, but in SFH4 the converse is true. Yet the distance modulus offsets are similar. The offsets are quite small and can be considered to be within the noise, but a possible reason could be the fact that Cole's method ignores the RGB and RC, so the distance is essentially an MS-fitting distance, while the Bologna method includes RGB and RC information. More interestingly, both distance estimates are shorter than recent determinations based on RR-Lyrae ($(m - M)_0 = 18.90$, Kapakos et al. 2011) and eclipsing binaries ($(m - M)_0 = 19.11$, North et al. 2010), but still compatible with the average distance of star clusters (around 18.87 for Glatt et al. 2008b and between 18.71 and 18.82 for Crowl et al. 2001). This variance may indicate a different sensitivity to reddening, which is highly variable across the SMC (see, e.g., Zaritsky et al. 2002; Haschke et al. 2011), or a line-of-sight depth effect (up to 4.9 kpc according to Subramanian & Subramaniam 2009, between 10 and 17 kpc according to Glatt et al. 2008b) which may depend on the direction.

The age–metallicity relations inferred by both methods are consistent, implying a metallicity slowly increasing with time and the bulk of the stars with metallicities between $0.001 \lesssim Z \lesssim 0.002$. The models derived with the Bologna procedure consistently find better fits when a metallicity of $Z = 0.008$

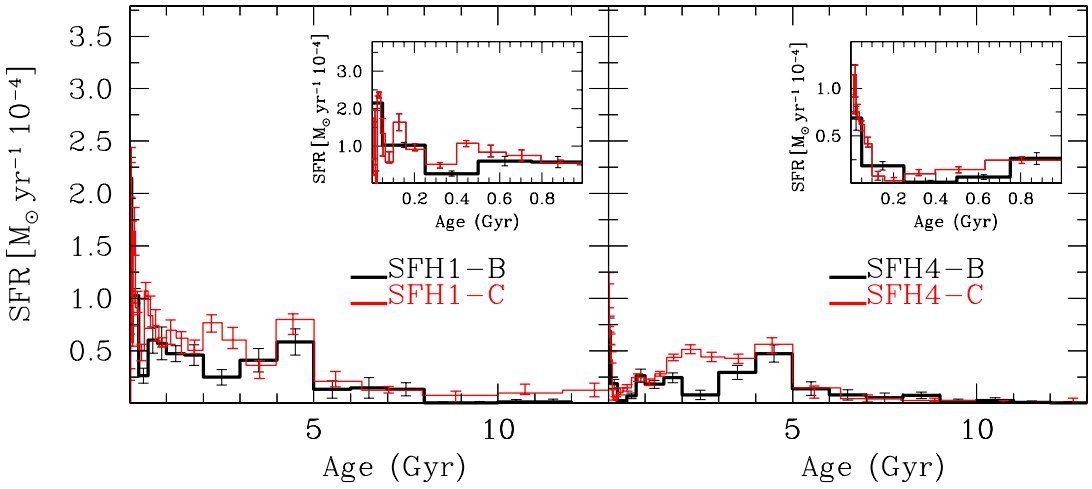


**Figure 20.** Bologna SFHs (black line) compared to Cole's (red line). The left panel and the right panel refer to the fields SFH1 and SFH4, respectively. The inset panels zoom in on the last 1 Gyr.

(A color version of this figure is available in the online journal.)

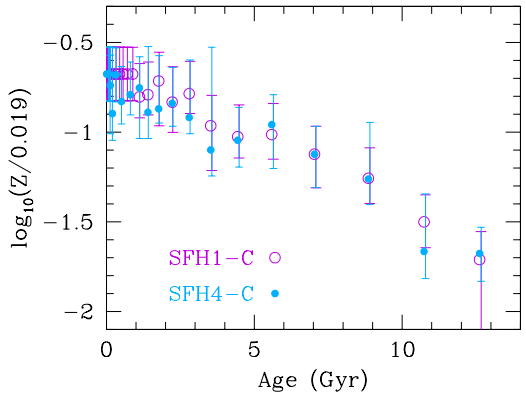


**Figure 21.** Best-fit age–metallicity relation of the two Bar fields derived by Cole's method. The two fields show similar chemical evolution; within the error bars they are the same. Taken together, they paint a consistent picture of average metallicity increasing steadily over time.

(A color version of this figure is available in the online journal.)

is included for the younger ages, while such a population is not required in Cole's models (see Figure 21). However, Cole adopted a higher differential reddening in his modeling of SFH1, which has the higher fraction of young stars; see Table 1.

### *4.4. Comparison between the Two Fields*

#### *4.4.1. Spatially Resolved SFH of the SMC Bar*

Direct comparison of the two fields shows that colors and magnitudes of the prominent stellar sequences are similar, and the main differences concern the younger stellar populations. In SFH1, the upper MS, BL, and red supergiant region are more populous, indicating a higher SFR at ages of a few hundred Myr or less. A challenge for both SFH-fitting methods was to reproduce the breadth of the upper MS in SFH1, as well as its RC, which was overproduced by both procedures. Integrating up the predicted stellar masses from the SFH-fitting procedures, we find that $\approx 4 \times 10^5$ $M_\odot$ stars formed over the lifetime of SFH1, and $2 \times 10^5$ $M_\odot$ in SFH4.

The general similarity of the two CMDs indicates that their features are representative of the general properties of the central SMC over most of its history. Small localized bursts/gasps of star formation may be smoothed away by the drifting of stars away from their birthplace except for the youngest ages. The dramatic increase in SFR at 5 Gyr is a strong feature in both fields and suggests a global change in environment to one that strongly favored star formation throughout the SMC at this time. Backward integration of the Magellanic Clouds orbital paths around each other and the Milky Way over this length of time are quite uncertain, and it is therefore difficult to say if this increase is associated with a tidal interaction or not.

More recent dynamical signatures should be easier to locate in time, and thus to correlate with global star formation events. Diaz & Bekki (2011) presented orbital calculations for the system MW/LMC/SMC, finding evidence for a close encounter about 1.5–2.0 Gyr ago. Analyzing SMC clusters, Piatti (2011) also suggested two enhanced formation processes that peaked at 2 and 5–6 Gyr ago. A comparison with our solutions suggests that the former episode might be associated with the Bologna (1.5 Gyr) and Cole (2.5 Gyr) intermediate-age peak, while the latter coincides with our strong rise 5 Gyr ago.

The inset panels in Figure 20 show the recent 1 Gyr history of both fields according to Bologna and Cole methods. In the SFH1 field, the mean specific SFR over the past 1 Gyr is nearly as high as the Gyr-averaged peak rate during the 5 Gyr event, but in SFH4 the recent SFR is reduced by a factor of $\approx 3$ from the intermediate-age peak. However, in both fields, the recent average specific SFR is still several times higher than the rate prior to the major episode 5 Gyr ago. The increase in the very youngest age bin may be an artifact of the fitting process, because the only stars younger than $\approx 50$ Myr in our CMDs are still on the MS—all of the evolved stars are above our bright limit—and so the code is free to vary the SFR at young ages somewhat arbitrarily to fit the residuals left after older populations are constrained. However, in literature, there are also reports indicating very recent bursts of activity; see, e.g., the analysis by Indu & Subramaniam (2011) who found peaks at 0–10 Myr and 50–60 Myr ago. Stars formed in these events, however, may not have had time to diffuse through the SMC, and thus may not be present in our two small *HST* fields.

There are also clear differences between the two fields, with SFH4 showing a lower overall SFR density averaging $\approx 5 \times 10^{-3}$ $M_\odot$ yr$^{-1}$ kpc$^{-2}$ and SFH1-forming stars at the average rate of $2.8 \times 10^{-2} M_\odot$ yr$^{-1}$ kpc$^{-2}$ with an apparently higher degree of burstiness. The features in the CMD that indicate high

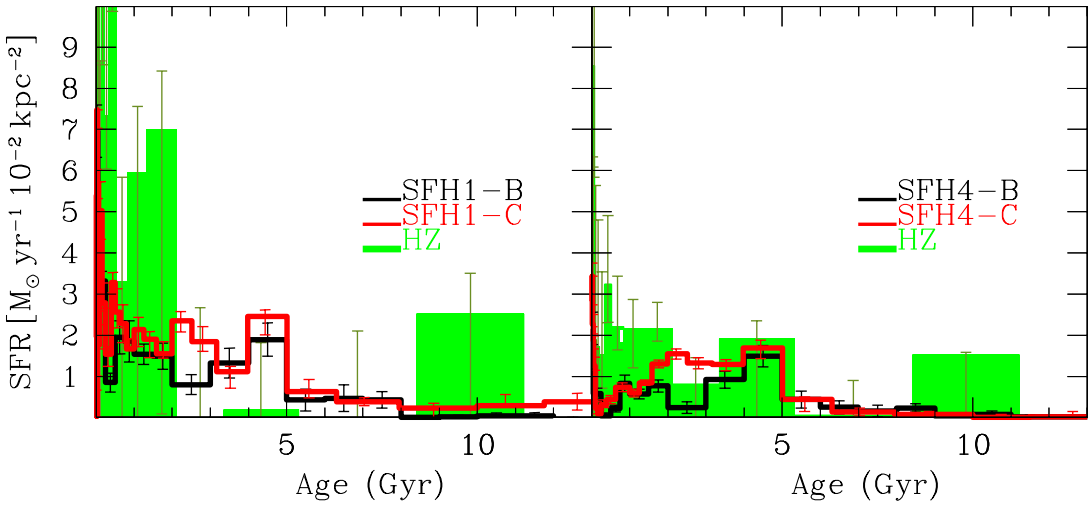


**Figure 22.** Comparison between our results (Bologna's solution is in black, Cole's is in red) and Harris & Zaritsky (2004) solutions (HZ) for SFH1 (left panel) and SFH4 (right panel).

(A color version of this figure is available in the online journal.)

SFR at the "burst" ages are the large number of MS stars at $I \approx 17$–17.5 (100–150 Myr) and the steepening of the MS LF at around $I \approx 19.5$–20, with the resulting large number of red core helium-burning stars (vertical RC; 400–800 Myr). In SFH1, the average recent SFR is comparable to the peak of the long-term average SFH since the 5 Gyr episode, but in SFH4 the rate has dropped by a factor of ≈3 from the peak. If it is proposed that a tidal interaction between the SMC and LMC (e.g., Besla et al. 2012) or Milky Way resulted in a period of increased SFR at 100–200 Myr as seen in SFH1, then it remains to be explained why this event is not seen in the SFH4 field.

#### 4.4.2. Chemical Evolution

Because a range of metallicities is considered at most ages, we can plot the resulting age–metallicity relation for the best-fit solutions. This is shown for the Cole solutions (which use a finer grid of metallicities, see Table 1) in Figure 21, which shows that the two fields have experienced similar long-term chemical evolution histories. This is not a surprising result because over time periods longer than $\sim 10^9$ yr the entire galaxy should be mixed, but it is a confirmation that the fit procedure is giving consistent results despite the differences between the two fields. For the youngest populations, only a single metallicity ($Z = 0.004$) has been used, so the error bars simply reflect the spacing of the metallicity grid. Where multiple metallicities were used, the mass-averaged mean metallicity is given, and the error bar shows the range of metallicities within which 90% of the stars in each age bin are expected to fall. The mean metallicity is quite similar to that obtained from the Bologna method results, with the exceptions that $Z = 0.008$ populations are not present in large numbers in the Cole solution, and the Bologna solution for SFH4 appears to increase its metallicity more quickly for ages older than ≈6 Gyr. Given the uncertainties in RGB model colors and the differences in distance and reddening between the two fits, it is not clear these differences are significant.

The field star AMR shown in Figure 21 is consistent with Piatti's (2012) AMR, whose AMR is obtained from CCD Washington CT1 photometry. Moreover, the metallicity values for ages older than 1 Gyr match well the spectroscopic field star measurements of red giants in the central SMC reported by Parisi et al. (2010).

Compared to AMRs derived from clusters, our result is in good agreement with Da Costa & Hatzidimitriou (1998) and Glatt et al. (2008b), while it differs from the cluster AMR of Piatti (2011) and Parisi et al. (2009). Piatti's (2011) metallicity dispersion is much higher than our formal errors at any age, suggesting that SMC clusters may have originated from a less mixed interstellar medium. Parisi et al.'s (2009) AMR rises faster than ours prior to 10 Gyr, suggesting that SMC clusters may have experienced an independent chemical evolution history.

It is worth reminding that we have derived the best AMRs from two small regions of the SMC and more fields are needed to confirm our results. A detailed comparison of our six AMRs (sampling regions of the Bar, Wing and Halo) with spectroscopic metallicity measurements will be presented in a future paper.

## 5. COMPARISON WITH OTHER STUDIES

Harris & Zaritsky (2004, hereafter HZ04) were the first to apply the synthetic CMD method to the derivation of the SMC SFH. They used wide-field UBVI photometry of an area of $4^\circ \times 4^\circ.5$ (MCPS catalog; Zaritsky et al. 2002), suggesting that 50% of SMC stars formed earlier than 8.4 Gyr ago, and that the period between 3 and 8.4 Gyr ago experienced very little, if any, star formation activity. Figure 22 shows HZ04's results for their regions including our SFH1 and SFH4 compared with our derivations. Both HZ04's solutions show a significantly higher stellar production prior to 8.4 Gyr ago. At intermediate ages, HZ04's solution for SFH1 is characterized by a clear and long lull between 2 Gyr and 8.4 Gyr ago, which is in striking contrast with our SFHs, whereas HZ04's SFH for SFH4 is stronger and in satisfactory agreement with our predictions. In the last 2 Gyr, both HZ04's SFRs are much stronger than our findings.

One should note that the HZ04 SFHs are derived from a much larger field of view (about 16 times wider) and their photometry did not reach the oldest MSTO. This last point is particularly relevant, since studies that do reach it indicate, instead, that, although present, stars older than 8 Gyr do not dominate the SMC population (Dolphin et al. 2001; McCumber et al. 2005; Noël et al. 2007, 2009; Chiosi & Vallenari 2007). Further support

to this is also provided by the relatively low number of RR Lyrae stars detected in the SMC compared to the LMC (Soszyñski et al. 2010).

Dolphin et al. (2001) analyzed an external region close to the globular cluster NGC 121, and concluded that stars in the outskirts of the SMC formed during a broadly peaked episode of star formation, with the largest rate between 5 and 8 Gyr ago. As expected, this outer field is significantly older than ours, although the contribution from the age bins older than 10 Gyr is again a minor fraction of the total mass produced.

McCumber et al. (2005) studied an external field in the SMC Wing, and found an increasing rate from 12 to 4 Gyr ago, and then over the past 1.5 Gyr, with a significantly quieter phase between 4 and 1.7 Gyr ago. This analysis was not conducted using a statistical significance testing and their favored solution was the one (among three ansatz models) which best matched the star counts in five strategic CMD regions. Although this makes the comparison with our finding difficult, two considerations can be made: (1) also in this case the stellar production prior to 10 Gyr ago is low, in agreement with our result; and (2) apart from a recent burst, the average activity of their SFH is earlier than in our fields, as expected for a Wing region, which represents a population with intermediate age between the Bar and the outskirts.

Noël et al. (2007) and Noël et al. (2009) produced one of the most extensive and accurate photometric campaigns in the SMC outskirts (see also Nidever et al. 2011). Their 12 fields are sufficiently deep to reach the old MSTO and none of them showed a clear extended HB, representative of a very old and metal-poor stellar population. Noël et al. (2009) used a population synthesis technique and recovered a great variety of SFHs, with only the outer fields characterized by a strong old and intermediate-age activity. Although the spatial distribution of these fields, mainly enclosed in the periphery of the SMC, makes the comparison with our results less direct, we note that among Noël et al.'s (2009) solutions, their innermost field (qj0112) most closely resembles our history of the Bar. Prior to 8 Gyr ago, the typical SFR density in their fields seems comparable with ours, suggesting that the SMC periphery and Bar share a common old population but that the initiation of significant star formation at 5–6 Gyr affected the Bar far more than the external regions of the SMC, marking the birth of the Bar as a distinct feature.

A more direct comparison can be made with Chiosi & Vallenari (2007), whose analysis was focused on three deep *HST*/ACS fields located in the Bar. In this case, our solutions are in good quantitative and qualitative agreement. All Chiosi & Vallenari's (2007) SFHs show both an unambiguous rise between 7 and 5 Gyr ago (with the precise epoch varying depending on the specific direction) and a negligible earlier activity. However, despite the low rate, their and our early activities are not zero, offering a natural explanation to the relatively low number of RR-Lyrae stars found in the SMC. Moreover, no two solutions are alike, suggesting that the SFR at young and intermediate ages was strongly variable across the SMC Bar.

Our results are rather similar to the SFHs of other two Local Group irregulars such as IC 1613 (Skillman et al. 2003) and Leo A (Cole et al. 2007): both galaxies show an initial quiet period followed by a prompt rise in the SF activity about 5–7 Gyr ago, with a peak between 3 and 6 Gyr and between 2 and 3 Gyr ago, respectively. In both cases, the recent activity (<2 Gyr ago) is more similar to that in SFH4 than in SFH1, presumably because the IC 1613 explored field is in the outskirt and the Leo A field is large enough to include central as well as peripheral regions.

Finally, comparing our SFH with the solutions found in the literature for the LMC (see, e.g., Harris & Zaritsky 2009 and Smecker-Hane et al. 2002), we find an overall similarity. Apart from the very early SF enhancement predicted by both Harris & Zaritsky and Smecker-Hane et al. that has no counterpart in our SMC solutions, our results for SFH1 share key properties with Smecker-Hane et al.'s (2002) findings for the LMC Bar: (1) a lull over the period 6–10 Gyr ago, (2) a steep increase at 5–6 Gyr, and (3) a gasping regime over the last 5 Gyr.

In spite of these similarities, the SMC and LMC AMRs (see, e.g., Carrera et al. 2008; Harris & Zaritsky 2009) remain rather different. While the LMC metallicity has increased faster both prior to 10 Gyr ago and over the last 4 Gyr (reaching [Fe/H] $\sim -0.7$ and [Fe/H] $= -0.2$, respectively), between these periods it has progressed at a much slower rate.

Moreover, it is well known that the LMC cluster distribution shows a long gap between 3 and 12 Gyr. If this gap is a consequence of the quiescent period between 6 and 10 Gyr ago (see, e.g., Harris & Zaritsky 2009), then it is intriguing that a similarly long quiescent period has no counterpart in the SMC cluster distribution (which has been steadily increasing with time).

## 6. SUMMARY AND CONCLUSIONS

This paper is the first of a series devoted to quantitative reconstruction of the SMC SFH from the deep *HST*/ACS observations presented in Sabbi et al. (2009). Here, we have explored the directions SFH1 and SFH4, both located in the SMC's Bar, by comparing the observational CMDs with a library of model CMDs incorporating photometric uncertainties and incompleteness as estimated by Sabbi et al. (2009). To provide a robust characterization of the SFH, the choice of the best model CMD was independently conducted with two objective statistical methods, namely Cole's (Cole et al. 2007) and Bologna's (Cignoni & Tosi 2010) procedures.

Our best-simulated CMDs exhibit an overall good agreement with observational CMDs. The star counts along the MS and the SGB morphology are generally well reproduced, indicating that our recovered SFHs and metallicity distributions are reasonable. However, while SFH4 CMD is well fitted, there are some difficulties to reproduce the exact morphology of SFH1's CMD, especially the upper-MS spread and RC counts, which are underestimated and overestimated, respectively. Concerning the resulting SFHs, a good consistency is found between the two methods in both fields. The only significant difference is the stronger rate suggested by Cole's SFH4 solution between 1.5 and 3 Gyr ago.

The combination of synthetic CMDs which most resembles the observations suggests the following picture. At early times, both fields experienced a long quiescent phase characterized by low SFRs, followed by a rapid SF increase around 5–6 Gyr ago. Since then, the mode of star formation has been somewhat different in the two fields. In SFH1, the star formation was gasping and reasonably high up to today. In SFH4, it was smoother and slowly declining.

To account for these differences and similarities, possible explanations are as follows.

*Recent burstiness.* The different level of burstiness is not surprising because these fields are separated by a distance (850 pc) larger than most of the star-forming complexes discovered in the

SMC (see Livanou et al. 2007), thus allowing the recent activity to fluctuate independently;

*Recent systematic behavior.* The stellar density in the SFH4 region is lower than in SFH1. Hence, the systematic decrease of SF activity in SFH4 may be connected with a minor amount of fuel available to support it up to today;

*Early quiescence and prompt rise.* Are the quiescent period and rapid SF increase 5–6 Gyr ago a global property of the Bar? Recent observations of RGB stars have revealed that older stellar components of the SMC have a velocity dispersion of about 27.5 km $s^{-1}$ (Harris & Zaritsky 2006), high enough to distribute the stars over a large distance (of the order of few kpc) from their birth places within few Gyr. Hence, the low early activity and the prompt rise are not peculiarities of our fields but global features of the SMC Bar. Moreover, Subramanian & Subramaniam (2012) find no evidence for a Bar in older stars, which is consistent with our low early activity. Further support is also provided by Chiosi & Vallenari (2007), who found similar star formation trends for three other Bar fields located around the SMC clusters K 29, NGC 290, and NGC 265. From the theoretical point of view, it is not clear what mechanism is responsible for the rapid rise of stellar production. Was it externally triggered by the MW or the LMC, or self-initiated? The striking similarity between the SMC and LMC SFH is suggestive of the former. Pointing in this direction are the recent calculations by Diaz & Bekki (2011) who presented evidence that around 5.5 Gyr ago the LMC and SMC were within 160 kpc of the MW and 200 kpc of each other, therefore arguing for an independent origin of the Clouds. In this scenario, the transition between quiescent and active phases could be naturally explained in terms of growing rate of mutual interactions started around 5 Gyr ago.

Finally, Rafelski & Zaritsky (2005) noted that the spatial distribution of the younger and older clusters in the SMC is statistically different, leading to the inference that a significant accretion or merger event may have taken place around 3–5 Gyr ago.

The study reported in this paper was the first step in a wider research activity aimed to characterize the SMC SFH through deep *HST*/ACS observations. A forthcoming paper will be dedicated to the analysis of the Wing and Halo fields. This will allow a comparative analysis to look for global physical characteristics in the SMC star formation process.

M.C. and M.T. have been partially funded with contracts COFIS ASI-INAF I/016/07/0 and ASI-INAF I/009/10/0. E.K.G. acknowledges partial funding from Sonderforschungsbereich "The Milky Way System" (SFB 881) of the German Research Foundation (DFG), especially via subproject A2. Partial support for JSG's analysis of data from *HST* program GO-10396 was provided by NASA through a grant from the Space Telescope Science Institute, which is operated by the Association of Universities for Research in Astronomy, Inc., under NASA contract NAS 5-26555.

## REFERENCES

Anderson, J., & King, I. R. 2006, Instrum. Sci. Rep. ACS 2006-01, 1
Anderson, J., Sarajedini, A., Bedin, L., et al. 2008, AJ, 135, 2055
Angeretti, L., Tosi, M., Greggio, L., et al. 2005, AJ, 129, 2203
Bertelli, G., Girardi, L., Marigo, P., & Nasi, E. 2008, A&A, 484, 815
Bertelli, G., Nasi, E., Girardi, L., & Marigo, P. 2009, A&A, 508, 355
Besla, G., Kallivayalil, N., Hernquist, L., et al. 2012, MNRAS, 421, 2109
Carlson, L. R., Sewiło, M., Meixner, M., et al. 2011, ApJ, 730, 78
Carrera, R., Gallart, C., Hardy, E., Aparicio, A., & Zinn, R. 2008, AJ, 135, 836
Cash, W. 1979, ApJ, 228, 939
Castellani, V., Degl'Innocenti, S., Girardi, L., et al. 2000, A&A, 354, 150
Chabrier, G. 2003, PASP, 115, 763
Chiosi, E., & Vallenari, A. 2007, A&A, 466, 165
Cignoni, M. 2006, PhD thesis, University of Pisa
Cignoni, M., Degl'Innocenti, S., Prada Moroni, P., & Shore, S. N. 2006, A&A, 459, 783
Cignoni, M., Sabbi, E., Nota, A., et al. 2009, AJ, 137, 3668
Cignoni, M., & Tosi, M. 2010, Advances in Astronomy, 158568
Cignoni, M., Tosi, M., Sabbi, E., Nota, A., & Gallagher, J. S. 2011, AJ, 141, 31
Cignoni, M., Tosi, M., Sabbi, E., et al. 2010, ApJ, 712, L63
Cole, A. A., Grocholski, A. J., Geisler, D., et al. 2009, in IAU Symp. 256, The Magellanic System: Stars, Gas, and Galaxies, ed. J. Th. van Loon & J. M. Oliveira (Cambridge: Cambridge Univ. Press), 263
Cole, A. A., Skillman, E. D., Tolstoy, E., et al. 2007, ApJ, 659, L17
Crowl, H. H., Sarajedini, A., Piatti, A. E., et al. 2001, AJ, 122, 220
Da Costa, G. S., & Hatzidimitriou, D. 1998, AJ, 115, 1934
Diaz, J. D., & Bekki, K. 2011, ApJ, 750, 36
Dolphin, A. E., Walker, A. R., Hodge, P. W., et al. 2001, ApJ, 562, 303
Duquennoy, A., & Mayor, M. 1991, A&A, 248, 485
Glatt, K., Gallagher, J. S., III, Grebel, E. K., et al. 2008a, AJ, 135, 1106
Glatt, K., Grebel, E. K., Gallagher, J. S., III, et al. 2009, AJ, 138, 1403
Glatt, K., Grebel, E. K., Jordi, K., et al. 2011, AJ, 142, 36
Glatt, K., Grebel, E. K., Sabbi, E., et al. 2008b, AJ, 136, 1703
Grebel, E. K., Roberts, W. J., & Brandner, W. 1996, A&A, 311, 470
Greggio, L., Tosi, M., Clampin, M., et al. 1998, AJ, 504, 725
Harris, J., & Zaritsky, D. 2004, AJ, 127, 1531
Harris, J., & Zaritsky, D. 2006, AJ, 131, 2514
Harris, J., & Zaritsky, D. 2009, AJ, 138, 1243
Haschke, R., Grebel, E. K., & Duffau, S. 2011, AJ, 141, 158
Haschke, R., Grebel, E. K., Duffau, S., & Jin, S. 2012, AJ, 143, 48
Indu, G., & Subramaniam, A. 2011, A&A, 535, A115
Kallivayalil, N., van der Marel, R. P., & Alcock, C. 2006, ApJ, 652, 1213
Kapakos, E., Hatzidimitriou, D., & Soszyński, I. 2011, MNRAS, 415, 1366
Kroupa, P. 2001, MNRAS, 322, 231
Livanou, E., Gonidakis, I., Kontizas, E., et al. 2007, AJ, 133, 2179
Mazeh, T., Goldberg, D., Duquennoy, A., & Mayor, M. 1992, ApJ, 401, 265
McCumber, M. P., Garnett, D. R., & Dufour, R. J. 2005, AJ, 130, 1083
Monelli, M., Hidalgo, S. L., Stetson, P. B., et al. 2010, ApJ, 720, 1225
Nidever, D. L., Majewski, S. R., Muñoz, R. R., et al. 2011, ApJ, 733, L10
Noël, N. E. D., Aparicio, A., Gallart, C., et al. 2009, ApJ, 705, 1260
Noël, N. E. D., Gallart, C., Costa, E., & Méndez, R. A. 2007, AJ, 133, 2037
North, P., Gauderon, R., Barblan, F., & Royer, F. 2010, A&A, 520, A74
Nota, A., Sirianni, M., Sabbi, E., et al. 2006, ApJ, 640, L29
Origlia, L., & Leitherer, C. 2000, AJ, 119, 2018
Parisi, M. C., Geisler, D., Grocholski, A. J., Claría, J. J., & Sarajedini, A. 2010, AJ, 139, 1168
Parisi, M. C., Grocholski, A. J., Geisler, D., Sarajedini, A., & Claría, J. J. 2009, AJ, 138, 517
Piatti, A. E. 2011, MNRAS, 418, L69
Piatti, A. E. 2012, MNRAS, 422, 1109
Rafelski, M., & Zaritsky, D. 2005, AJ, 129, 2701
Ripepi, V., Marconi, M., Musella, I., et al. 2006, Mem. Soc. Astron. Ital., 9, 267
Sabbi, E., Gallagher, J. S., Tosi, M., et al. 2009, ApJ, 703, 721
Salpeter, E. E. 1955, ApJ, 121, 161
Sirianni, M., Jee, M. J., Benítez, N., et al. 2005, PASP, 117, 1049
Skillman, E. D., & Gallart, C. 2002, in ASP Conf. Ser. 274, Observed HR Diagrams and stellar evolution, ed. T. Lejeune & J. Fernandes (San Francisco, CA: ASP), 535
Skillman, E. D., Tolstoy, E., Cole, A. A., et al. 2003, ApJ, 596, 253
Smecker-Hane, T. A., Cole, A. A., Gallagher, J. S., III, & Stetson, P. B. 2002, ApJ, 566, 239
Soszyński, I., Udalski, A., Szymański, M. K., et al. 2010, Acta Astron., 60, 165
Subramanian, S., & Subramaniam, A. 2009, A&A, 496, 399
Subramanian, S., & Subramaniam, A. 2012, ApJ, 744, 128
Tolstoy, E., Hill, V., & Tosi, M. 2009, ARA&A, 47, 371
Tosi, M., Gallagher, J. S., III, Sabbi, E., et al. 2008, in IAU Symp. 255, Low-Metallicity Star Formation: From the First Stars to Dwarf Galaxies, ed. L. K. Hunt, S. Madden, & R. Schneider (Cambridge: Cambridge Univ. Press), 381
Tosi, M., Greggio, L., Marconi, G., & Focardi, P. 1991, AJ, 102, 951
Udalski, A., Soszyński, I., Szymański, M. K., et al. 2008, Acta Astron., 58, 329
Zaritsky, D., Harris, J., Thompson, I. B., Grebel, E. K., & Massey, P. 2002, AJ, 123, 855